Climatology of Significant Tornadoes within China and Comparison of Tornado Environments between the United States and China

CHENYUE ZHANG,[a] MING XUE,[a,b,c] KEFENG ZHU,[a,d] AND XIAODING YU[e]

[a] *Key Laboratory of Mesoscale Severe Weather, Ministry of Education, School of Atmospheric Sciences, Nanjing University, Nanjing, Jiangsu, China*
[b] *Center for Analysis and Prediction of Storms, University of Oklahoma, Norman, Oklahoma*
[c] *School of Meteorology, University of Oklahoma, Norman, Oklahoma*
[d] *Key Laboratory of Transportation Meteorology of China Meteorological Administration, Nanjing Joint Institute for Atmospheric Sciences, Nanjing, China*
[e] *China Meteorological Administration Training Center, Beijing, China*

(Manuscript received 14 March 2022, in final form 7 October 2022)

ABSTRACT: A climatology of significant tornadoes [SIGTOR, tornadoes rated (E)F2+ on the (enhanced) Fujita scale] within China and in three subregions, including northern, central, and southern China, is first presented for the period 1980–2016. In total, 129 SIGTOR are recorded in China, with an average of 3.5 per year. The tornado inflow environments of the south-central and southeast regions of the United States (USC and USSE) are compared with those of China and its subregions based on sounding-derived parameters including shear, storm-relative helicity, convective available potential energy (CAPE), lifting condensation level (LCL), etc. Soundings are extracted from the ERA5 reanalysis dataset. The results confirm that the SIGTOR in USSE are characterized by high shear, low CAPE, and low LCL whereas those in USC are characterized by moderate-to-high shear, high CAPE, and high LCL. The thermodynamic conditions of tornadic cases are favorable for China, with moderate-to-high CAPE and low-to-moderate LCL, but their kinematic conditions are much less favorable than in the United States, a fact that is believed to be primarily responsible for the lower tornado frequency and intensity in China. The high CAPE in China is due mostly to high humidity. For three subregions in China, the central China cases account for 60% of total samples, and its environmental features are similar to those of China. The average shear with northern China cases is stronger than that with the other two subregions, and the midlayer is relatively dry. The southern China SIGTOR have the most conducive humidity conditions, but the CAPE and shear there are the lowest. The northern, central, and southern China environments can be considered as representative of midlatitude, subtropical, and tropical regions.

SIGNIFICANCE STATEMENT: We document the climatological characteristics of significant tornadoes (SIGTOR) within China and compare the inflow environments of SIGTOR in China and its subregions with those in the U.S. central and southeastern regions. The availability of hourly high-resolution ERA5 data makes the environments based on extracted proximity soundings much more accurate than possible with earlier reanalyses. The environmental characteristics show systematic differences in the tornado environments of different regions of China and the United States and suggest different roles played by thermodynamic and kinematic conditions for tornado formation. Overall, the environmental differences are consistent with the resulting frequency and intensities of SIGTOR. The findings are helpful toward improving tornado forecasting and warning or even understanding of potential impacts of climate change on SIGTOR, especially in China, where such studies are rarer.

KEYWORDS: Tornadoes; Climatology; Storm environments

1. Introduction

The United States is the country with the most tornadoes in the world, with more than 1000 cases and approximately 50 significant tornado [SIGTOR, tornadoes rated (E)F2 or greater on the (enhanced) Fujita scale] events occurring annually (Henson 2003; Grams et al. 2012). Although China and the United States are located in a similar latitudinal zone and both have higher terrains in the western part of the country, the total number of tornadoes in China (~108 per year) is about one-tenth that of the United States, and significant cases amount to only 3.3 per year (Fan and Yu 2015; Chen et al. 2018). Despite the few numbers, when SIGTOR do occur, as they have in recent years (Xue et al. 2016; Zhao et al. 2017; Meng et al. 2018), their damage can be enormous. Differences in the environmental conditions of the two countries can likely explain the differences in the frequency of tornado occurrences in the regions, but detailed studies on tornado environments in China are still lacking so far.

There have been a number of studies investigating the effectiveness of sounding-derived parameters in distinguishing storm types and forecasting tornado occurrence in the United States (Rasmussen and Blanchard 1998; Thompson et al. 2003, 2014; Craven and Brooks 2004; Grams et al. 2012; Sherburn and Parker 2014; Anderson-Frey et al. 2016; Reames 2017). Soundings extracted from gridded analysis datasets are often used to study effects of tornado environments, including

Corresponding author: Ming Xue, mxue@ou.edu

DOI: 10.1175/MWR-D-22-0070.1

derived parameters. In general, tornadoes tend to form in environments with high vertical wind shear, large convective instability and abundant low-level moisture. Wind shear plays an important role in maintaining and enhancing convective storms by reducing precipitation interruption to updraft and inducing dynamic vertical pressure gradient force, thus, organized strong storms are more likely to occur in environments with higher shear (Weisman and Klemp 1982; Markowski and Richardson 2011). Further, low-level storm-relative helicity (SRH) can significantly enhance updraft rotation when horizontal streamwise vorticity is ingested into the storm and tilted to the vertical in updraft (Davies-Jones 1984; Lilly 1986; Davies-Jones et al. 1990). Recent work of Coffer et al. (2019) suggests that SRH integrated within a shallower near-surface layer has increasing forecast skill, suggesting that the lower-level kinematic conditions are more important to the formation of low-level mesocyclones as well as tornadoes.

Convective available potential energy (CAPE) is a commonly used parameter to measure environment instability, and CAPE values above 1000 J kg^{-1} are considered to be moderate to high (Rasmussen and Blanchard 1998, hereinafter RB98). Convective inhibition (CIN) and temperature lapse rates are also parameters related to stability. With high CAPE, low CIN, and low lifting condensation level (LCL), the probability of tornado occurrence increases (Markowski et al. 2002; Thompson et al. 2003). More than one-half of SIGTOR in RB98 have LCLs below 800 m. In addition, combined parameters including bulk Richardson number (BRN), energy-helicity index (EHI), vorticity generation parameter (VGP), supercell composite parameter (SCP), and significant tornado parameter (STP) have been devised to include contributions of kinematic and thermodynamic components and they usually show a better ability in discriminating storm types and tornadogenesis potential (Rasmussen and Blanchard 1998; Rasmussen 2003; Thompson et al. 2003, 2011).

The U.S. Great Plains and the southeastern United States are two regions prone to SIGTOR (Kelly et al. 1978; Brooks et al. 2003; Henson 2003; Coleman and Dixon 2014; Krocak and Brooks 2018; Anderson-Frey et al. 2019). For the Great Plains, peak tornado activity occurs during early May in Oklahoma and Texas (Brooks et al. 2003). In more recent years, tornadoes in the southeastern regions of the United States have received much attention (Rasmussen et al. 2017). Many tornadoes in this region occur in the cold season and at night, under favorable kinematic but less favorable thermodynamic conditions that feature high shear and low CAPE as compared with the high-shear and high-CAPE conditions in the Great Plains (Kis and Straka 2010; Davis and Parker 2014; Sherburn and Parker 2014; Sherburn et al. 2016; Long et al. 2018; Anderson-Frey et al. 2019). In the southeastern United States, high shear, low CAPE severe events typically occur in moist boundary layers within the warm sector or along the cold front of a strong surface cyclone and are characterized by strong synoptic-scale forcing with strong upstream vorticity maximum at 500 hPa, strong low-level warm-air advection, and a surface cyclone centered north of the severe events (Sherburn et al. 2016).

Fan and Yu (2015) documented the climatology of tornadoes in China from 1961 to 2010. There were 165 SIGTOR recorded in the period, with 3.3 cases annually on average. Topographically, most tornadoes occurred in regions associated with flat terrain and seasonally they were more likely to occur in spring and summer, peaking in the afternoon and evening. Chen et al. (2018) extended the time period of tornado climatology to 65 years (1948–2012). Considering both weak and strong tornadoes, they estimated that about 108 tornadoes occurred per year in China on average. They showed that tornadoes were mainly distributed in eastern China, especially in coastal provinces, consistent with the finding of Fan and Yu (2015). In terms of the synoptic background, North China (midlevel) cold vortex, mei-yu frontal system, and tropical cyclone (TC) are three main synoptic backgrounds for tornadoes in China. The tornado cases within the cold vortex systems feature low low-level humidity, and the TC tornadoes feature relatively low CAPE, whereas mei-yu systems provide the most favorable background environment for tornadoes (Zheng 2020).

Few studies have examined the environmental parameters associated with tornadic storms in China. Some recent studies on tornadoes of China have emphasized the general characteristics of tornadic storms and tornado damages for individual cases (Xue et al. 2016; Zheng et al. 2016; Bai et al. 2017; Zhao et al. 2017; Meng et al. 2018). Bai et al. (2020) found that TC tornadoes tend to be spawned in environments characterized by large SRH and large E-CAPE (entraining CAPE). Yu et al. (2021) compared environmental parameters of tornadic and nontornadic supercells in China from 2002 to 2016 using nearby radiosondes that had to be modified using ground station data because of timing differences. Their study suggested that tornadic supercells of the study period on average had weaker instability, more water vapor and significantly higher low-level shear than nontornadic supercells. Based on a 10-yr tornado record, Zhou et al. (2021) compared the environments of tornado-prone seasons in tornado-active regions of the United States and China and suggested that tornadoes in China had favorable thermodynamic but less favorable kinematic conditions relative to those in the United States. Their study did not examine environmental conditions of actual tornado events, however. Because of the lack of systematic studies on tornado environments, in terms of specific environmental parameters, the experimental tornado forecasting carried out by the weather bureaus of China generally borrow from U.S. tornado research and operational forecasting practices.

Because SIGTOR are responsible for most tornado deaths and are more likely to have been documented in the climatological records than weaker tornadoes (Concannon et al. 2000), we focus on SIGTOR in this study. Based on a 37-yr (1980–2016) record, the climatologies of SIGTOR within China and in three subregions of China are first presented. Analyses of near-storm soundings are then performed, seeking to identify differences of tornado environments among China and two representative tornado-prone regions in the United States, that is, the central Great Plains and southeast United States. The environmental parameters are calculated

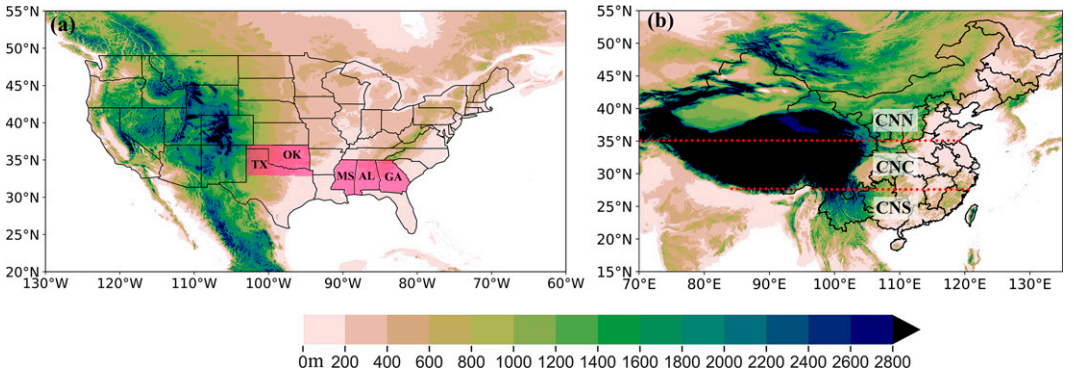

FIG. 1. (a) Central United States (USC) and southeastern United States (USSE). Pink shadings denote the two regions. USC includes Oklahoma (OK) and north of Dallas, Texas (TX), and USSE includes Mississippi (MS), Alabama (AL), and Georgia (GA). (b) Boundaries of northern (CNN), central (CNC), and southern China (CNS). The two red dashed lines represent the 35° and 27.5°N latitude lines, respectively.

from soundings extracted from the tornadic storm (based on tornado report locations) inflow regions from the ERA5 reanalysis data (Hersbach et al. 2020) that are available every hour. The latter is important to ensure that the environment sampled is close to the time of tornadic event while most earlier tornado environment studies were limited by the low temporal resolution of reanalysis or observed sounding data. This current study can potentially provide guidance to forecasters in predicting SIGTOR potential in China.

The rest of this paper is organized as follows. Section 2 presents the methods and data used in this study. Sections 3 and 4 present and discuss the results of SIGTOR climatology and tornado environmental parameters and their statistical distributions, respectively. A summary and conclusions are given in section 5.

2. Data and methods

a. Study regions, sounding extraction, and environmental parameters

As mentioned earlier, the Great Plains and the southeastern United States are two regions of high tornado risk. In light of previous works (Kelly et al. 1978; Coleman and Dixon 2014) and considering that the selected regions for comparison should be similar in size, we choose the central U.S. area (denoted hereinafter USC) that consists of the state of Oklahoma and the part of Texas north of Dallas, along with the southeastern U.S. region (denoted hereinafter USSE) that includes the states of Mississippi, Alabama, and Georgia (see Fig. 1a). The U.S. tornado reports, accessed via the National Oceanic and Atmospheric Administration Storm Prediction Center (NOAA/SPC), are used for the intensity rating, start time, start location, and path of each tornado. We mainly consider China as a whole given the much smaller number of SIGTOR in China while at the same time we also examine SIGTOR within three subregions of China, which are divided by latitude lines 35° and 27.5°N into northern, central, and southern China (see Fig. 1b). No SIGTOR was recorded in the west part of China where terrain is complex; thus the three subregions only include parts of the eastern portion of the country. These subregions tend to be primarily influenced by midlatitude, subtropical, and tropical weather systems, respectively, in the warm season after the onset of Asian monsoon. Before the onset of Asian monsoon, northern and central China are mainly influenced by midlatitude systems and southern China is mostly influenced by subtropical weather.

Information on tornadoes is obtained from the "The Collection of Meteorological Disasters Records in China" (Ding 2008) as well as from reports found on the Internet, but the EF scales are not given in these sources. Yu et al. (2021) determined the EF scales of tornadoes according to damage indicators of the U.S. National Weather Service survey standard. In the records, the description of tornado is often not sufficiently detailed, and when in doubt the lower scale is typically chosen. For example, if there is uncertainty in the judgment of EF2, it is generally determined to be EF1. Standardized tornado damage surveys were not commonly carried out in China until 2012 (Zheng et al. 2016; Bai et al. 2017; Meng et al. 2018; Cai et al. 2021), although such surveys are not always complete. Because EF0/1 tornadoes are more difficult to record accurately, we only consider SIGTOR in this study. For both countries, SIGTOR records spanning a 37-yr period from 1980 to 2016 are included in the statistics.

A total of 129 SIGTOR in China were recorded in the 37 years, averaging 3.5 per year, whereas there are 796 and 616 reports in USSE and USC, averaging 21.5 and 16.6 per year, respectively. It is worth noting that no (E)F5 tornado was reported and only 3 (E)F4 cases occurred during the period in China. Eighty cases occurred in central China, accounting for 62% of the total in China, and there are more stronger [(E)F3 or greater] tornadoes reported in central China (15) than in northern China (only 1) and southern China (2) (see Table 1). The limited number of cases in northern China and southern China may lead to unreliable statistical results.

The fifth-generation ECMWF reanalysis (ERA5) dataset that is available every hour is used to extract tornado proximity soundings. Previous studies usually use 3- or 6-hourly reanalysis

TABLE 1. Numbers of SIGTOR classified by regions and ratings. The total and annual average numbers of SIGTOR in each region are also shown; CN, CNN, CNC, and CNS are abbreviations of China, northern China, central China, and southern China, respectively.

Region	(E)F2	(E)F3	(E)F4	(E)F5	No. of SIGTOR	Annual avg No.
CN	111	15	3	0	129	3.5
CNN	24	0	1	0	25	0.7
CNC	65	13	2	0	80	2.2
CNS	22	2	0	0	24	0.6
USSE	553	194	41	8	796	21.5
USC	433	143	36	4	616	16.6

datasets or radiosonde observations at even coarser temporal resolutions for proximity soundings, which may be off by 3 h or more in timing relatively tornado start time. With the hours proceeding tornado occurrence, significant changes in environmental conditions can occur (Novlan and Gray 1974; Maddox 1976; McCaul 1991; Brooks et al. 1994; Kerr and Darkow 1996; Rasmussen and Blanchard 1998; Craven and Brooks 2004). Apart from the high (hourly) temporal resolution that can keep the timing errors of proximity soundings to within one hour, another important advantage of ERA5 is its superior horizontal (0.25°) resolution with 37 pressure levels in the vertical. Taking advantage of the high temporal and vertical resolutions of the ERA5 dataset, Coffer et al. (2020) and Taszarek et al. (2020) recently investigated the environments of severe convective weather including tornadoes over the United States and Europe.

In this study, we apply the proximity-inflow method of RB98 to help determine the locations of proximity sounding extractions relative to tornado reports. In RB98, observed soundings at 0000 UTC were used, and the proximity-inflow method was used to associate each severe weather event with an observed sounding. In their case, a sounding was assumed to be in the inflow sector of any severe weather event if it was within 400 km and the event fell within ±75° of the wind vector averaged within the lowest 500 m AGL, and such a sounding was assumed to be associated with the event. The main issue with their study was that the soundings were available only at one time (0000 UTC) and the soundings are sparse; the soundings selected may be too far (representing large-scale environment rather than storm environment) or too close (may be convectively contaminated) to the storm and therefore not very representative of the storm environment (Thompson et al. 2003; Potvin et al. 2010). With the 0.25° hourly ERA5 data, most of the problems can be avoided. Potvin et al. (2010) found that soundings within 40–121 km and 0–1 h of the tornadoes best represent the tornadic storm environment. The method we use in this paper is briefly described below.

1) Step 1: Assign the environmental conditions at the closest hourly time prior to the event.
2) Step 2: Assemble a list of all ERA5 grid points that are within 100 km of the event, as in RB98 but with a smaller distance.
3) Step 3: As in RB98, assemble a subset of grid point soundings that contain the event in a "±75°" sector centered along the direction of boundary layer mean (averaged over 500 m AGL) inflow wind vector, choose the grid point with the maximum CAPE, and mark this point as point A.
4) Step 4: We take point A as the center and select the points that satisfy the inflow conditions from the top, bottom, left, right of point A and point A itself, to do an average that results in the sounding that we will use to represent the inflow environment of each SIGTOR event. This step is added to avoid unrealistic extreme values of CAPE.

b. *Environmental parameter computations and analysis techniques*

Each sounding associated with SIGTOR is used to calculate 17 severe storm parameters that have been used to diagnose severe weather potential in previous severe weather studies. The computing methods and abbreviations are shown in Table 2. The Sounding and Hodograph Analysis and Research Program in Python (SHARPpy), an open-source sounding analysis program including the routines that are as consistent as possible with the methods developed at NOAA/SPC (Blumberg et al. 2017), is used to calculate the parameters. Virtual temperature correction is applied to thermodynamic computations (i.e., CAPE, CIN, and LCL) (Doswell and Rasmussen 1994). If not specified, CAPE, CIN, LCL are computed based on parcel lifted from the 100-hPa mixed layer (Craven et al. 2002). We discard the sounding samples with CAPE equaling 0 J kg^{-1}. From 1980 to 2016, there were 11 TC tornadoes in China (including 6 in central China and 5 in southern China), accounting for a high proportion of the total number of SIGTOR in China. Since TC tornado environments are very different, we removed the TC tornadoes from the China cases. In the United States, TC tornadoes accounts for only 3.4% of all tornadoes according to Schultz and Cecil (2009), which has very small impact on the mean environment therefore we did not attempt to remove them. Discussions of section 4 are based on 93 China (SIGTOR in China without exact time were also removed), 790 USSE, and 609 USC cases, with some parameters presented for subregions of China. The average distances of the extracted soundings from the storm reports are 75.0, 79.2, and 75.2 km, respectively, for China, USSE, and USC.

The relative relationships of parameters in different regions can be better visualized with box-and-whisker plots. The boxes contain the middle 50% of the events, and the median is shown with a horizontal line. The vertical bar contains the middle 80% of the events. Since subjective comparison of distributions (e.g., visual inspection of box-and-whisker plots) does not account for sample size, a nonparametric statistical significance test, permutation test (Efron and Tibshirani 1993), is used to identify differences between the parameter distributions in different regions. In addition, to better show the clustering of tornado environments in two-dimensional spaces of severe weather sounding parameters, a smoothing technique known as kernel density estimation (KDE) is employed (Zucchini 2003). KDE assigns each data point a

TABLE 2. References and equations for the severe parameters calculated for this study. Here, **V** denotes an environment wind, with a subscript indicating the layer (AGL) where this value was taken. For SRH, **C** denotes the storm motion vector and **k** is the unit vector pointing upward. Here, T_v denotes virtual temperature (°C), with additional subscripts p, e, and b denoting a value associated with a lifted parcel, the environment, and an average temperature for the layer, respectively. LFC stands for a lifted parcel's level of free convection, EL stands for its equilibrium level, and z_i stands for its initial level. The u_{avg} denotes the difference between the density-weighted mean wind in low-level (0–500 m) and midlevel (0–6 km). MU and SB indicate most unstable and surface-based layer, respectively, and E denotes effective inflow parcel layer. EBWD and ESRH denote effective bulk shear and effective SRH, respectively.

Parameter	Formula/method	Reference
0–1-km shear (SR1km)	$\text{SR1km} = \mathbf{V}_{\text{1km}} - \mathbf{V}_{\text{sfc}}$	Thompson et al. (2003)
0–6-km shear (SR6km)	$\text{SR6km} = \mathbf{V}_{\text{6km}} - \mathbf{V}_{\text{sfc}}$	Thompson et al. (2003)
0–1-km storm-relative helicity (SRH1)	$\text{SRH1} = -\int_0^{\text{1km}} \mathbf{k} \cdot (\mathbf{V} - \mathbf{C}) \times \frac{\partial \mathbf{V}}{\partial z}\, dz$	Davies-Jones et al. (1990)
0–3-km storm-relative helicity (SRH3)	$\text{SRH3} = -\int_0^{\text{3km}} \mathbf{k} \cdot (\mathbf{V} - \mathbf{C}) \times \frac{\partial \mathbf{V}}{\partial z}\, dz$	Davies-Jones et al. (1990)
Convective available potential energy (CAPE)	$\text{CAPE} = g\int_{\text{LFC}}^{\text{EL}} \left(\frac{T_{vp} - T_{ve}}{T_{ve}}\right) dz$	Moncrieff and Miller (1976)
Convective inhibition (CIN)	$\text{CIN} = g\int_{z_i}^{\text{LFC}} \left(\frac{T_{ve} - T_{vp}}{T_{vb}}\right) dz$	Colby (1984)
850–500-hPa lapse rate	$850-500\text{-hPa LR} = -\left(\frac{\text{T}_{\text{500hPa}} - \text{T}_{\text{850hPa}}}{\text{z}_{\text{500hPa}} - \text{z}_{\text{850hPa}}}\right)$	Thompson (2020)
700–500-hPa lapse rate	$700-500\text{-hPa LR} = -\left(\frac{\text{T}_{\text{500hPa}} - \text{T}_{\text{700hPa}}}{\text{z}_{\text{500hPa}} - \text{z}_{\text{700hPa}}}\right)$	Thompson (2020)
Lifted condensation level (LCL)	Solved iteratively	Stackpole (1967)
Surface–850-hPa relative humidity (lowRH)	Mean relative humidity over the lowest 150 hPa	Blumberg et al. (2017)
850–700-hPa relative humidity (midRH)	Mean relative humidity over a layer 850–700 hPa	Blumberg et al. (2017)
Bulk Richardson No. (BRN)	$\text{BRN} = \text{CAPE}/[0.5(u_{\text{avg}})^2]$	Weisman and Klemp (1982)
Energy-helicity index (EHI)	$\text{EHI} = \frac{\text{CAPE} \times \text{SRH1}}{1.6 \times 10^5}$	Hart and Korotky (1991), Davies (1993)
Vorticity generation parameter (VGP)	$\text{VGP} = \frac{\int_0^{\text{h}} \left\lvert \frac{\partial \mathbf{V}}{\partial z} \right\rvert dz}{\int_0^{\text{h}} dz} \times \text{CAPE}^{1/2}$	Rasmussen and Blanchard (1998)
Supercell composite parameter (SCP)	$\text{SCP} = \underbrace{\left(\frac{\text{MUCAPE}}{1000\ \text{J kg}^{-1}}\right)}_{\text{cape term}} \times \underbrace{\left(\frac{\text{ESRH}}{50\ \text{m}^2\ \text{s}^{-2}}\right)}_{\text{srh term}} \times \underbrace{\left(\frac{\text{EBWD}}{20\ \text{m s}^{-1}}\right)}_{\text{bwd term}}$	Thompson et al. (2011)
Significant tornado parameter (STP)	$\text{STP} = \underbrace{\left(\frac{\text{SBCAPE}}{1500\ \text{J kg}^{-1}}\right)}_{\text{cape term}} \times \underbrace{\left(\frac{2000 - \text{SBLCL}}{1000\ \text{m}}\right)}_{\text{lcl term}} \underbrace{\left(\frac{\text{SRH1}}{150\ \text{m}^2\ \text{s}^{-2}}\right)}_{\text{srh term}} \times \underbrace{\left(\frac{\text{BWD6}}{20\ \text{m s}^{-1}}\right)}_{\text{bwd term}}$	Thompson et al. (2003)
Significant tornado parameter with CIN (STPC)	$\text{STPC} = \underbrace{\left(\frac{\text{CAPE}}{1500\ \text{J kg}^{-1}}\right)}_{\text{cape term}} \times \underbrace{\left(\frac{\text{CIN} + 200}{150\ \text{J kg}^{-1}}\right)}_{\text{cin term}} \times \underbrace{\left(\frac{2000 - \text{LCL}}{1000\ \text{m}}\right)}_{\text{lcl term}} \times \underbrace{\left(\frac{\text{ESRH}}{150\ \text{m}^2\ \text{s}^{-2}}\right)}_{\text{srh term}} \times \underbrace{\left(\frac{\text{EBWD}}{20\ \text{m s}^{-1}}\right)}_{\text{bwd term}}$	Thompson et al. (2011)

shape known as a "kernel" that is a standardized weighting function centered on the location of its corresponding data point in the parameter space. Summing the kernels across the entire domain will create smooth transitions between densities (Anderson-Frey et al. 2016). Here a Gaussian kernel is used. We implement KDE with function gaussian_kde from python package scipy that includes automatic smoothing constant determination.

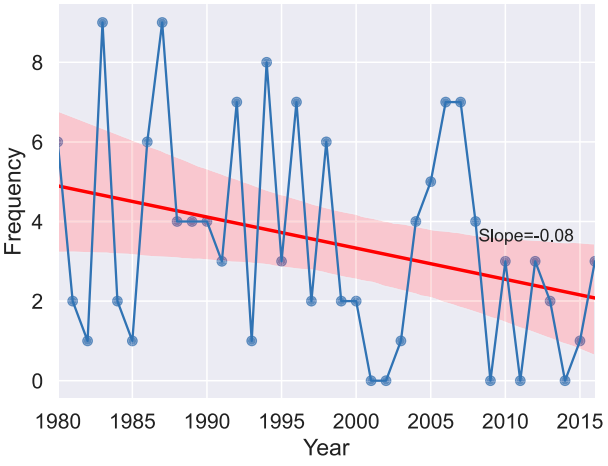

FIG. 2. Variation of the numbers of SIGTOR with year in China. The blue line denotes annual number of SIGTOR, the red line denotes the linear regression line, and the red shading denotes a 95% confidence interval. The slope of the regression line is labeled.

3. Significant tornado climatology

a. *Temporal distributions*

Figure 2 shows the annual SIGTOR numbers in China from 1980 to 2016, which do not exceed 10, and the numbers reach 7 to 9 in several years before 2009 but do not exceed 3 after 2009. Several years, including 2001, 2002, 2009, 2011, and 2014, do not have any SIGTOR reported. In general, the negative slope (−0.08) of linear regression indicates a slightly decreasing trend in this period, which is probably related to the fact that changes in the vertical wind shear and LCL in these years are not favorable for tornado formation.

Seasonal and diurnal variations in SIGTOR occurrence in China and the United States are depicted in Fig. 3. Consistent with works by Chen et al. (2018) and Fan and Yu (2015), SIGTOR in China are most prevalent in summer and spring, peaking in July and April, with rare SIGTOR activities from autumn through early spring (November–February) (Fig. 3a). Three (E)F4 tornadoes occurred in April, June, and July each, the high incidence months. Northern and central China both have two peaks in summer and spring, whereas southern China peaks in April with a slight secondary peak in August. The peak in July coincides with the arrival of summer monsoon in central China region when mei-yu season is ongoing. The central and southern China peaks in April, in which 27% of southern China cases occur, correspond to the South China rainy season when the summer monsoon reaches southern China (Wang and Li 2007). For northern China, SIGTOR are most active from May to September, corresponding to the start of the warm season in late spring and the northward migration of precipitation zones into North China in August. The peak in July is likely related to summer thunderstorm activities in the region (Fig. 3a).

The seasonal characteristics of USSE (Fig. 3c) and USC (Fig. 3e) SIGTOR are distinctly different. In USSE, most events occur from late autumn through the following spring, peaking in April and November, with relatively few SIGTOR activities in summer (Fig. 3c), which shows the same bimodal annual distribution as found in Long et al. (2018). The SIGTOR in USC mainly occur in spring and early summer and peak in May, with a much lower secondary peak in October, showing a stronger seasonal cycle. In this study, we define October–March of the next year as the cold season and the rest of the year as the warm season. Cold-season cases therefore account for 5%, 56%, and 19% of the total number of cases in China, USSE, and USC, respectively. For USC, most SIGTOR are associated with supercell storms that are most active in spring, whereas in USSE many tornadoes are associated with mesoscale convective systems such as quasi-linear convection (Trapp et al. 2005).

The exact time of 26 tornado events in China is not included in historical records; thus the number of SIGTOR used for diurnal analysis is smaller. Figure 3b shows an overall peak between 1600 and 1700 Beijing standard time (BJT; UTC + 8 h) with most SIGTOR occurring between early afternoon and early evening. The peak of southern China occurs 1 h earlier than those of central and northern China. Among the 3 (E)F4 tornadoes, 2 occurred between 1600 and 1700 BJT and 1 between 1400 and 1500 BJT (Fig. 3b).

USC also has a prominent afternoon peak, but it occurs later than that in China (Fig. 3f). The maximum frequency occurs at 1800–1900 central standard time (CST; UTC − 6 h), and most SIGTOR occur between 1500 and 2100 CST, that is, from late afternoon through early evening. There are very few SIGTOR after midnight and through the morning (Fig. 3f). In contrast, SIGTOR in USSE have a weaker diurnal cycle, with SIGTOR occurring at all times of the day. The frequency is highest between 1500 and 1900 eastern standard time (EST; UTC − 5 h), and there is a secondary high-frequency period between 0100 and 0500 EST that is believed to be associated with development of nocturnal low-level jet that enhances low-level wind shear and moisture transport (Markowski and Richardson 2011). About 72%, 56%, and 75% of SIGTOR occur in the daytime for China, USSE, and USC, respectively, where daytime is defined from 0800 to 2000 local time. About 28%, 44%, and 25% of SIGTOR occur at night for China, USSE, and USC, respectively. SIGTOR in USSE, which are comparatively more likely to occur during cool season and at night, bring more challenges to the public and forecasters because of nighttime occurrence and association with variable storm types (Ashley et al. 2008; Guyer and Dean 2010; Sherburn and Parker 2014).

b. *Spatial distributions of China tornadoes*

The geographic distribution of the SIGTOR of China (Fig. 4a) shows that the vast majority of the events occur in eastern regions of China where terrain is relatively flat, concentrating around the lower reaches of Yangtze–Huaihe Rivers (Jiangsu and Anhui provinces and Shanghai, labeled JS, AH, and SH in Fig. 4a), the North China Plains (Hebei, Henan, and Shandong provinces and Beijing, labeled HeB, HeN, SD, and BJ) and around Hubei and Hunan Provinces (HuB and HuN). Other cases are spread around Guangdong (GD) coastal area in southern China and the Northeast Plains [Liaoning (LN), Jilin (JL), and Heilongjiang (HLJ) provinces]. Tornadoes rated (E)F3 mainly occur in the Yangtze–Huaihe

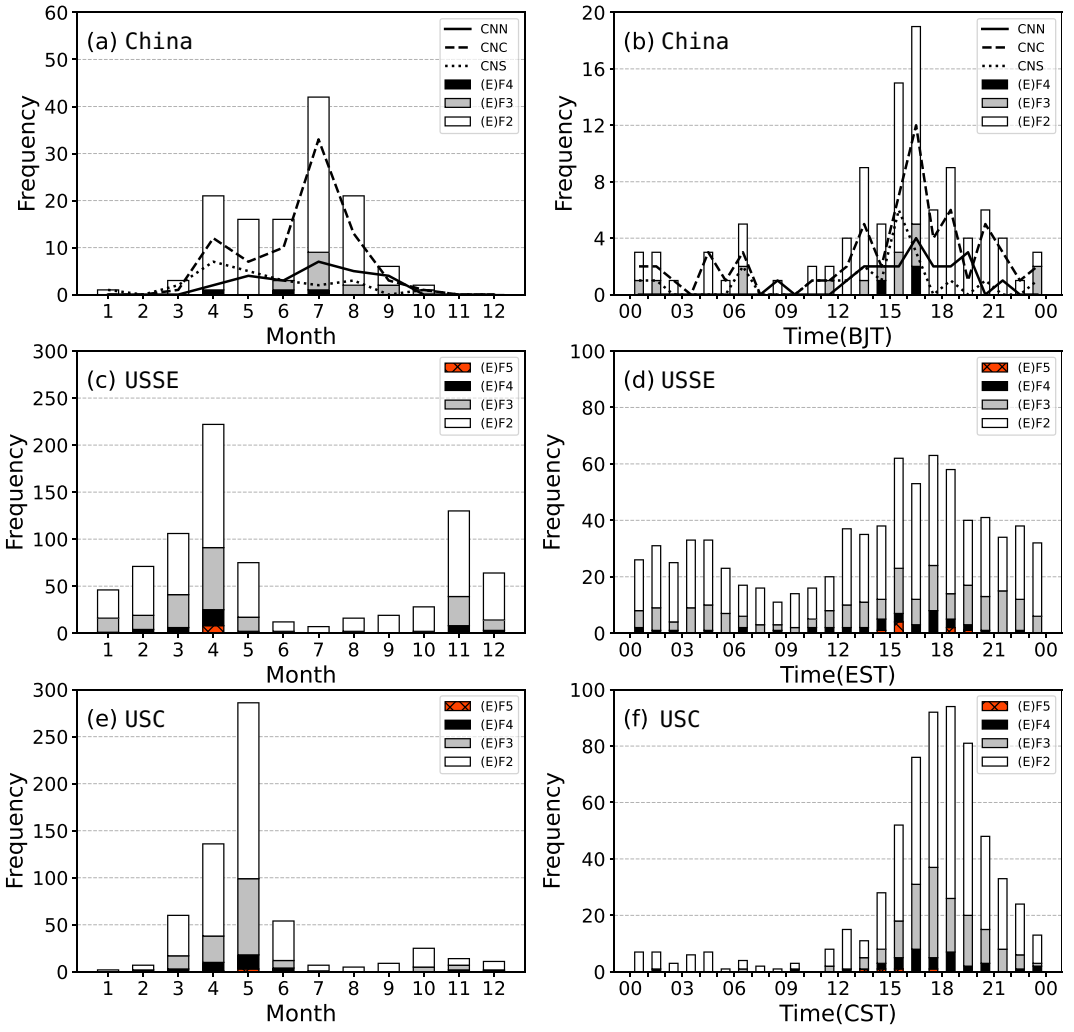

FIG. 3. Monthly variation of the number of SIGTOR in (a) CNN (solid line), CNC (dashed line), and CNS (dotted line), with the white, light-gray, and black bars denote frequency of SIGTOR rated (E)F2, (E)F3, and (E)F4; (c) USSE, with the orange-red "*x*" bar denoting frequency of tornadoes rated (E)F5; and (e) USC. Also shown is the diurnal variation of the number of SIGTOR in (b) China (Beijing time), (d) USSE (U.S. eastern standard time), and (f) USC (U.S. central standard time).

region, and the three (E)F4 cases occurred in Jiangsu, Hunan, and Heilongjiang provinces, respectively. Jiangsu (28), Guangdong (13) and Hunan (12) are the three provinces with the highest number of (E)F2 + tornadoes during the 37 years (Fig. 4b). The (E)F2 tornado reported in Inner Mongolia (InM) appears to be an exception in terms of terrain elevation (Fig. 4a). In general, SIGTOR are more likely to form over plains, as in the Great Plains of the United States and central and eastern plains of China, where strong low-level flows can more easily develop and maintain and moisture is plentiful.

4. Environmental parameter distributions

a. Kinematic parameters

For the 0–1-km shear, SR1km, northern China has a median of 10.4 m s^{-1} while central China has a median of 9 m s^{-1} (Fig. 5a). In comparison, more than 90% of the SIGTOR in southern China have SR1km values lower than 9 m s^{-1}. CNN–CNS and CNC–CNS are two pairs with sample mean differences supported by permutation test p values lower than 5% (≥95% confidence) among China subregions, suggesting that the low-level shear is significantly lower in southern China than other two subregions (Table 3). The differences in 0–6-km shear (SR6km) are similar to those of SR1km in the three subregions, with a slightly lower median for southern China and a slightly higher median for northern China; the relative differences are smaller (Fig. 5c). Because of the mountainous terrain in southern China, the shear layer above sea level is higher and therefore some of the overall synoptic shear may be lost by having a higher base elevation. Wang et al. (2015) investigated 13 tornado cases in northeast China from 2002 to 2013 and concluded that strong low-level and midlevel jet resulted in greater low-level (0–1 km)

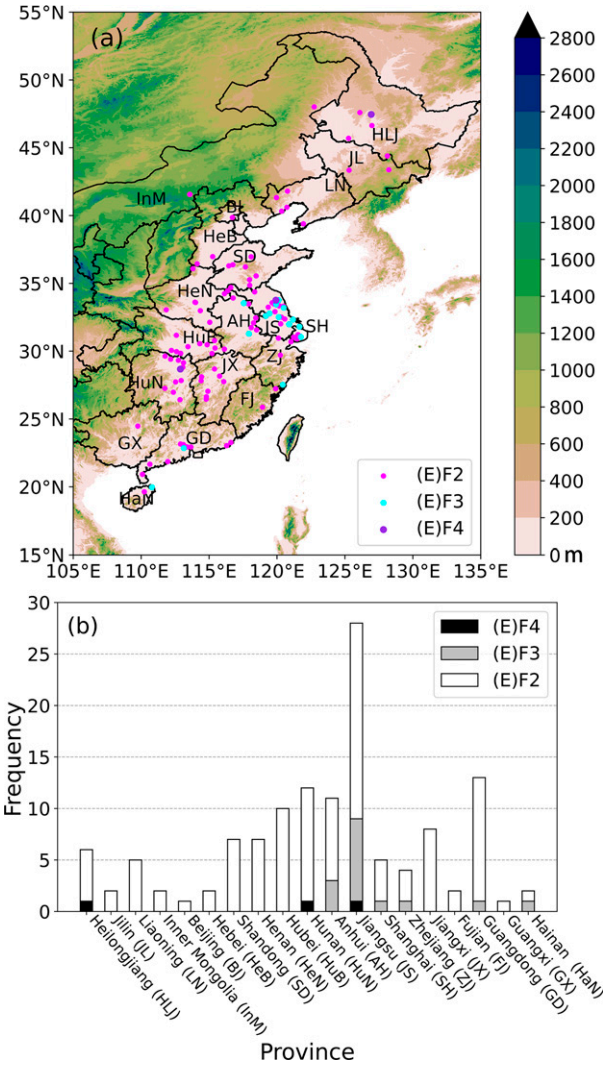

FIG. 4. Spatial distribution of SIGTOR: (a) terrain distribution; magenta, cyan, and violet dots denote (E)F2, (E)F3, and (E)F4 tornadoes, respectively, and (b) distribution by province. Shadings are as in Fig. 3.

and deep-level (0–6 km) shear at mean of 11.8×10^{-3} and 4.4×10^{-3} s^{-1}, in agreement with the ranges given here. SIGTOR in central China accounts for 60% of China samples, therefore, shows similar parameter distributions with China. SR1km and SR6km in China are lower than those in USSE and USC, especially when compared with USSE, which has the largest shear magnitude. The lower quartile (14.7 m s^{-1}) of the USSE SR1km is greater than the upper quartile (14.6 m s^{-1}) of USC and greater than the 90% quartile (13.8 m s^{-1}) of China. Although to a lesser degree than SR1km, USSE SR6km is also greater than northern China and USC (Fig. 5c).

Figure 6 shows composite hodographs for China and the two U.S. regions. To avoid too much smoothing of wind profiles when the deep layer shears have very different orientations, we realign the 0–6-km shear vectors before composite averaging. This was done by first averaging all sounding data for each of the three regions to obtain "raw" composite hodographs, as shown in dashed black lines in Fig. 6. The hodographs of individual soundings are then rotated so that their 0–6-km shear vectors are aligned with the 0–6-km shear vector of the raw composite hodograph. Composite averaging is then performed on the rotated hodographs. Such shear-aligned composite hodographs are shown in solid blue lines in Fig. 6. Similar hodograph compositing procedures have been used in previous studies (e.g., Brown 1993; Nixon and Allen 2022). Here we choose to keep the hodographs within the ground-relative framework since the ground-relative wind speed has implication for frictional effect on near surface shear, and we avoid uncertainties with the determination of storm motion in the case of storm-relative hodographs. The final and raw versions of the hodographs are actually similar, indicating that most individual hodographs have similar orientations for each region.

All composite hodographs for all three regions show clear clockwise curvature at the low levels, and the curvature is mostly in the lowest 1 km AGL. When compared with China and USC, the proportion of nighttime SIGTOR in USSE is higher and under the influence of nocturnal low-level jet (LLJ) the low-level vertical wind shear of USSE (over 20 m s^{-1} below 1 km) is the highest among three regions (Bluestein 2013; Reames 2017). USC low-level shear is smaller (about 5 m s^{-1} lower; Fig. 6c) than that of USSE whereas that of China is another 5 m s^{-1} weaker (Fig. 6a). Although with a larger degree of veering of the wind profile, the magnitude of deep-layer maximum wind speed in China is almost one-half of that in USSE, and is also smaller than that in USC; most of the differences are established below 6 km AGL (Fig. 6), confirming the importance of 0–6-km shear in addition to that of 0–1-km shear.

The mean SR1km and SR6km of different regions as a function of tornado rating are shown in Figs. 5b and 5d. Limited by the sample size, we do not show results of subregions of China. For both SR1km and SR6km, the China cases have the weakest shear for each tornado intensity scale, and the shear magnitude is generally 10 m s^{-1} lower than USSE for both SR1km and SR6km. Note that in Fig. 5b, the SR1km mean values of China are close to those of USC, especially for stronger tornadoes, while the SR6km mean values of China in each EF bin are about 5 m s^{-1} less than those of USC.

The low-level storm-relative helicity (SRH; Davies-Jones et al. 1990) is another important predictor of supercells and tornadoes, and it measures the amount of streamwise environmental vorticity that can be ingested into the storms that can then be turned into the vertical and induce strong updraft rotation (see calculation formula in Table 2). Integration over 1- and 3-km depths yield SRH1 and SRH3, respectively. Strongly curved hodographs at the low levels with large radius yield large SRH (cf. Fig. 6). Expectedly, the relative distributions of SRH shown in box-and-whisker plots and the mean values in line charts are similar to those of shears (Fig. 7). The SRH1 magnitude of China SIGTOR is around 40–150 m^2 s^{-2}, with a mean of 103 m^2 s^{-2} and the SRH3 magnitude is around 80–220 m^2 s^{-2} with a mean of 170 m^2 s^{-2}. In Thompson et al. (2003), 81% significantly tornadic supercells were associated with SRH1 $>$ 75 m^2 s^{-2}, and 90% of them had SRH3 $>$ 100 m^2 s^{-2}. Only 59% and 69% China samples meet or exceed

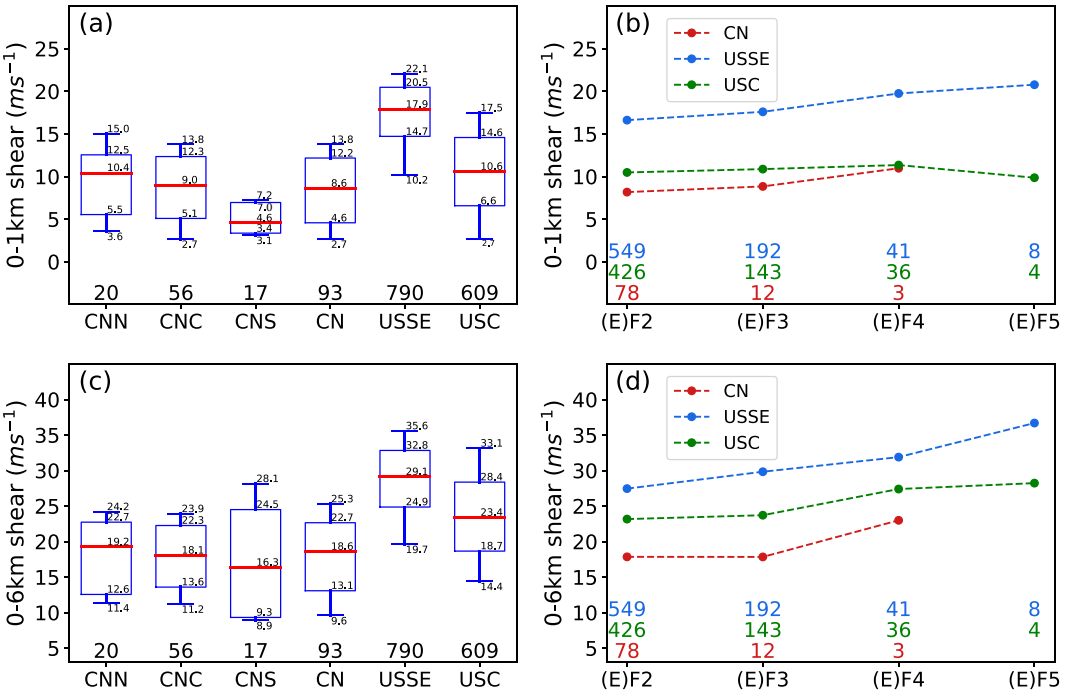

FIG. 5. Box-and-whisker graph of (a) SR1km, and (c) SR6km associated with SIGTOR in CNN, CNC, CNS, CN, USSE, and USC. The red line inside each colored box indicates the median value for that category, the limits of the box are the 25th and 75th percentiles, and the whiskers extend to the 10th and 90th percentiles. The numbers of samples for each group are listed below the columns. Also shown is the variation of the mean of (b) 0–1-km shear and (d) 0–6-km shear with tornado damage ratings. Red, blue, and green lines denote CN, USSE, and USC, respectively. The numbers of samples for each of the EF ratings for CN (red), USSE (blue), and USC (green) are listed below the columns.

the corresponding thresholds, whereas the percentages for USC and USSE are respectively 74% and 93% and 94% and 96%.

The p values obtained in tests indicate that there are significant differences of kinematic conditions among the three examined regions (Table 3). Recent work by Zhou et al. (2021) explained the apparently lower tornado numbers from a seasonal perspective. They found the wind speeds at 6 km AGL in all three regions resulting from the weakening of

TABLE 3. Mean parameter values of each region and results from permutation of means testing for all pairs of comparison groups. Permutation test statistics are given (%). Variables for which no test resulted in a significant test statistic are not shown. Influenced by extreme maxima, the mean of BRN is not representative and not listed here.

Parameter	CNN mean	CNC mean	CNS mean	CNN–CNC p (%)	CNN–CNS p (%)	CNC–CNS p (%)	CN mean	USSE mean	USC Mean	CN–USSE p (%)	CN–USCp (%)	USC–USSE p (%)
SR1km (m s^{-1})	9.61	8.91	5.42		0.48	0.25	8.44	17.04	10.65	≤0.02	≤0.02	≤0.02
SR6km (m s^{-1})	17.94	18.58	18.11				18.36	28.37	23.63	≤0.02	≤0.02	≤0.02
SRH1 (m^2 s^{-2})	125.29	108.47	56.44		0.77	1.17	102.70	259.61	157.46	≤0.02	≤0.02	≤0.02
SRH3 (m^2 s^{-2})	202.57	173.11	122.87		3.46		170.32	338.50	274.49	≤0.02	≤0.02	≤0.02
MLCAPE (J kg^{-1})	1733.17	1786.48	1509.29				1725.66	979.53	2200.21	≤0.02	≤0.02	≤0.02
MLCIN (J kg^{-1})	42.94	32.74	30.79				34.54	25.99	65.36	2.93	≤0.02	≤0.02
850–500-hPa LR (°C km^{-1})	6.87	6.18	6.18	≤0.02	0.62		6.33	6.39	7.22		≤0.02	≤0.02
700–500-hPa LR (°C km^{-1})	6.67	6.00	6.12	0.03	3.95		6.16	6.26	7.21		≤0.02	≤0.02
MLLCL (m AGL)	967.05	944.57	833.68				929.46	618.68	1091.76	≤0.02	0.08	≤0.02
lowRH (%)	79.68	79.74	83.63				80.43	91.65	75.90	≤0.02	0.29	≤0.02
midRH (%)	68.25	76.88	75.77	1.31			74.86	79.54	67.98	0.14	≤0.02	≤0.02
EHI1	1.20	1.08	0.49		0.75	1.59	1.00	1.54	2.00	≤0.02	≤0.02	≤0.02
VGP	0.16	0.15	0.11		0.98	1.95	0.15	0.18	0.21	0.05	≤0.02	≤0.02
SCP	7.11	7.07	3.54			2.77	6.44	8.28	12.51	0.41	≤0.02	≤0.02
STP	1.54	1.66	0.66		2.45	1.01	1.46	1.85	2.38	1.84	≤0.02	≤0.02
STPC	1.29	1.21	0.63				1.12	1.88	2.10	≤0.02	≤0.02	2.35

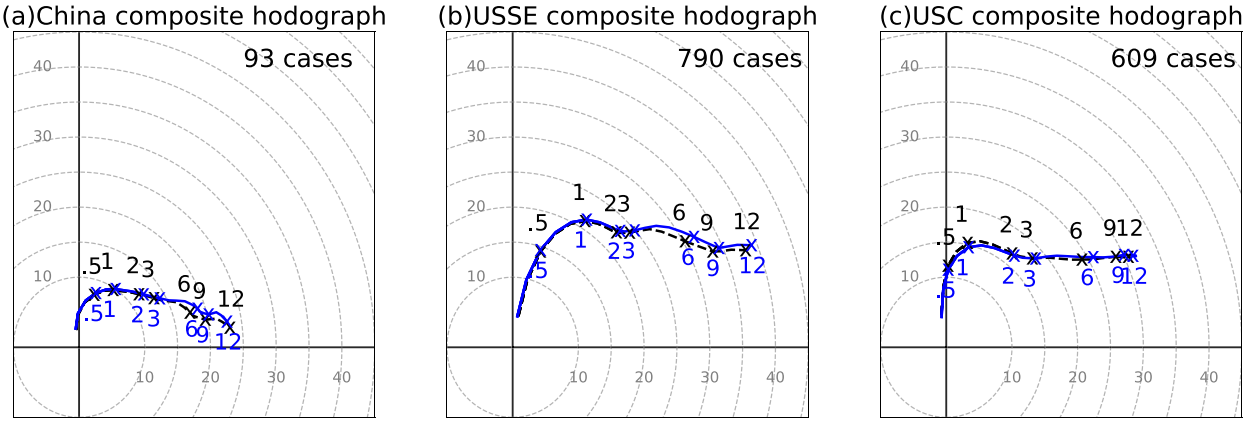

FIG. 6. Composite hodographs of (a) CN (93 cases), (b) USSE (790 cases), and (c) USC (609 cases) before (dashed black) and after (solid blue) 0–6-km shear vector realignment. Labels on the curves denote the height above ground level (AGL) in kilometers. For the shear-vector-realigned hodographs, composite averaging is performed after the 0–6-km shear vector of individual soundings is realigned with the mean 0–6-km shear vector. The wind speed unit is meters per second.

westerlies and the poleward movement of jet streams have analogous decreasing trends with month (March–August). The concentration of China SIGTOR in July (Fig. 3) corresponds to kinematic environment that is less favorable. Earlier in the year when the jet stream is located farther south, low level thermodynamic conditions under the primary influence of winter monsoon are, on the other hand, unfavorable.

b. *Thermodynamic parameters*

The CAPE and CIN for all regions are shown in Fig. 8. The median value of CAPE for China is 1732 J kg^{-1}, close to those of northern and central China. The median CAPE of southern China is a little lower at 1660 J kg^{-1} (Fig. 8a). USC has the highest CAPE among the three main regions, with a median of 2233 J kg^{-1} while that of USSE is 894 J kg^{-1}, much lower than both USC and China. USSE has a larger number of nocturnal tornadoes whose environments are characterized by decreased near-surface temperatures and by near surface inversion, leading to less instability (Reames 2017). The high CAPE in USC is often helped by energy accumulation within the boundary layer when it is capped by boundary layer top inversion. This is reflected by the highest CIN for USC among all regions (Fig. 8c).

In general, CAPE $>$ 1000 J kg^{-1} is regarded as large. Nearly 75% of cases in China meet this standard, indicating

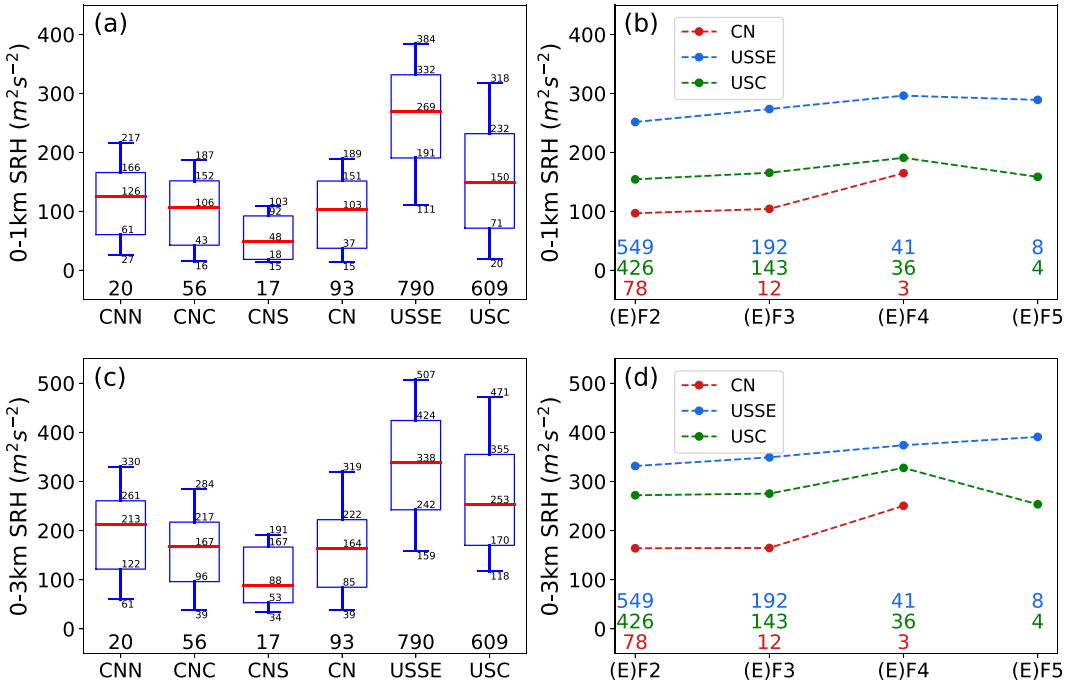

FIG. 7. As in Fig. 5, but for SRH1 and SRH3.

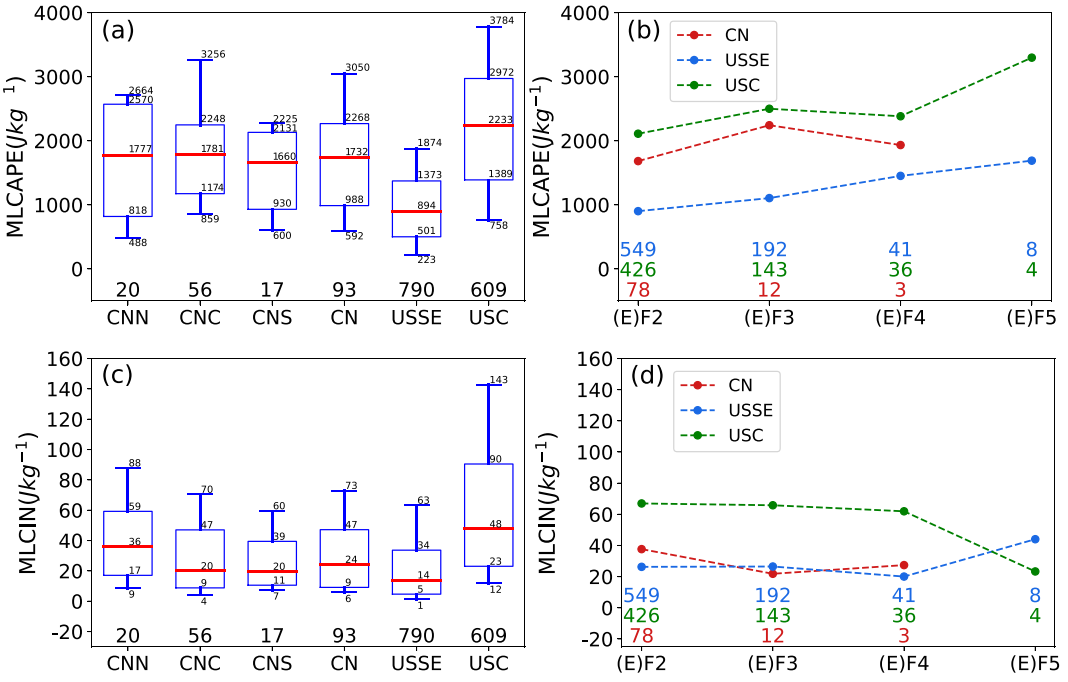

FIG. 8. As in Fig. 5, but for MLCAPE and MLCIN.

generally favorable instability conditions of the storm inflow. The mean value of China CAPE in each tornado rating is uniformly moderate, and 400–500 J kg^{-1} lower than those of USC, with a slightly increasing trend with the rating (Fig. 8b). In general, CAPE increases with increasing tornado intensity, with the increase being the largest for USC; the mean CAPE for (E)F5 tornadoes in USC is larger than 3000 J kg^{-1} while that of USSE is less than 1700 J kg^{-1}.

Another commonly examined parameter is CIN, which represents the energy needed to overcome negative buoyancy to achieve storm initiation. Northern China have larger CIN than central and southern China, likely due to its drier environment (Fig. 8c). The median value of China is 24 J kg^{-1}, slightly larger than that of USSE (14 J kg^{-1}) and the median CIN value of USC is the highest at 48 J kg^{-1}. While CIN is generally unfavorable for convection, the presence of CIN can help suppress unorganized convection or too quick convective initiation. In the afternoon, CAPE increases with surface heating. When CIN is eventually overcome, more CAPE tends to be available to the initiated convection.

The mid- to lower-level temperature lapse rate is another parameter measuring static stability. The 850–500- and 700–500-hPa lapse rates are used by NOAA/SPC (Garner 2012; Hurlbut and Cohen 2014) to discriminate between tornadoes associated with different synoptic backgrounds or various classes of report magnitude and we examine these two parameters here also. The relative distributions of 850–500-hPa lapse rates in different regions are similar to those of 700–500 hPa (Figs. 9a,c). Steeper lapse rates of northern China than those of central and southern China indicate greater instability there, which is in agreement with Wang et al. (2015), who found that the lapse rate is greater for northeast China tornadoes relative to those of tornadoes in the Yangtze–Huaihe region and in southern China. The median value for central China is slightly lower than that for southern China (Figs. 9a,c). Influenced by warm and dry midlevel air advected from the New Mexico plateau at around 1 km AGL (Carlson et al. 1983), the lapse rates in the USC region tend to be steeper relative to China and USSE. This is also the main reason that USC CAPE values are larger than those of China. Classifying lapse rate exceeding 7°C km^{-1} as steep, only 10% of China and USSE cases occur in steep lapse rate background, while USC has more than 50% of cases occurring in such environment (Figs. 9a,c). Also, for each tornado intensity scale, the USC cases have the steepest mean lapse rate, while those of China and USSE are comparable and lower (Figs. 9b,d).

The LCL as well as low-level and midlevel relative humidity are also examined. The average LCL of SIGTOR in different regions are 967 m (northern China), 945 m (central China), 834 m (southern China), 929 m (China), 619 m (USSE), and 1092 m (USC), respectively. Under the condition of similar surface temperature, lower LCL suggests more low-level water vapor giving rise to greater CAPE, which are consistent with the relative distribution of CAPE (Table 3; Figs. 10a,c,e and 8). In comparison with instability and shear, humidity is the most important favorable factor for SIGTOR in southern China, but in the absence of strong wind shear (cf. Fig. 5), supercells are rare there. In contrast, the water vapor conditions in the northern China region with low-level and midlevel humidity median values of 81.9% and 70.8% are less favorable among the three subregions, but the shear condition is most favorable (Fig. 5).

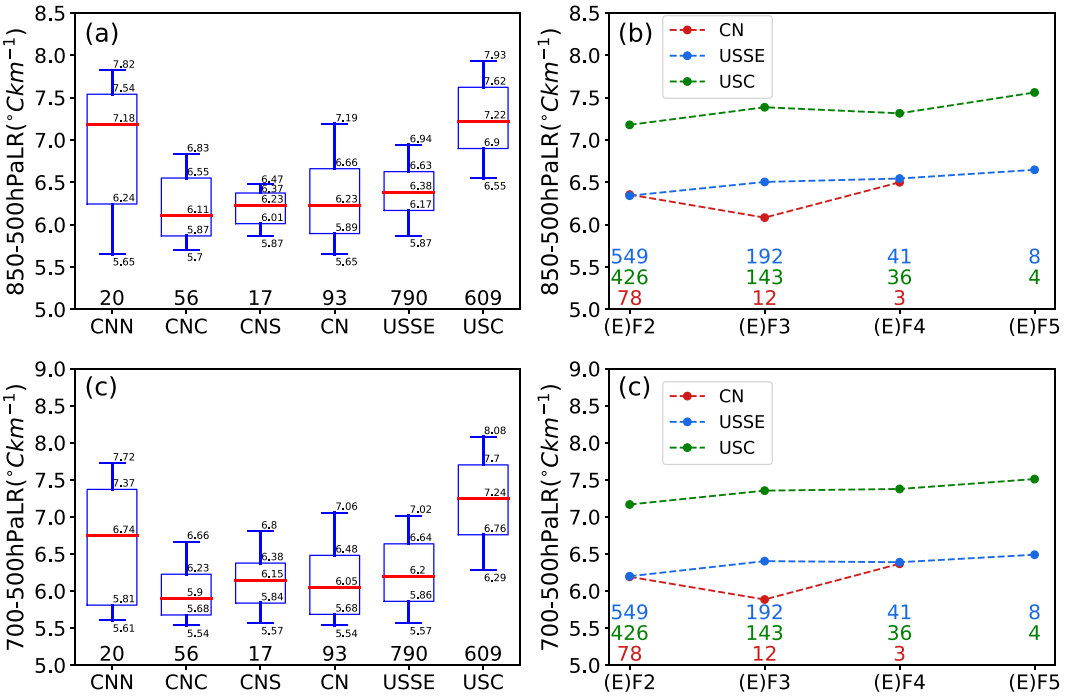

FIG. 9. As in Fig. 5, but for 850–500- and 700–500-hPa lapse rates.

There are large differences among the distributions of LCL in China, USSE, and USC. As expected, USSE that is close to the ocean shows the moistest environment with lowest LCL. In total 90% of the USSE samples having MLLCL < 900 m and the mean and median values of surface to 850-hPa average relative humidity are above 90% (Figs. 10c,d). The distributions of humidity-related parameters in northern China are closest to those of USC. Overall, the SIGTOR in China have favorable humidity conditions due to the Asian summer monsoon that transports moisture from South China Sea and Indian Ocean. In total 75% of the China events occur in environment with LCL < 1078 m, approximately 100 m lower than the upper quartile given by RB98 (1180 m) and Thompson et al. (2003) (1149 m). From Figs. 10b,d,f, we find that stronger China tornadoes tend to occur in more humid environments but such trends are less evident in USSE and USC in the figures.

Figure 11 shows the composite soundings for China, USSE, and USC regions for the SIGTOR. Though composite soundings are subject to smoothing effect, the most important features are retained. The SIGTOR environments of China are warm and moist, the environments of USSE are relatively cold and moist while the environments of USC are warm and relatively dry. These are consistent with the fact that most SIGTOR of China occur in the afternoon, USSE has a larger number of nocturnal tornadoes and most SIGTOR of USC occur in late afternoon and early evening. The soundings of China are characterized by moderate humidity and CAPE and relatively low vertical wind shear; the USSE soundings have high low-level relative humidity, low CAPE, and high wind shear while USC soundings are characterized by drier midlevel troposphere, high CAPE, and moderate-to-high wind shear (Fig. 11). Relatively large positive area on the skew T diagram extends to highest levels among the three in USC, supporting deep intense convection (Fig. 11c).

c. *Composite parameters*

In this section, bulk Richardson number (BRN), energy-helicity index (EHI), and vorticity generation parameter (VGP) related to the combinations of shear and CAPE, as well as supercell composite parameter (SCP) and significant tornado parameter (STP) combining multiple parameters (Table 2) are examined for different regions.

BRN was originally proposed by Weisman and Klemp (1982) as the ratio of CAPE and BRN shear, showing the balance of outflow and inflow (Table 2). Their study suggests that a BRN value of 10–50 is supportive for supercells. For BRN > 50, outflow will overwhelm the inflow leading to short-lived cells; BRN < 10, the shear is too strong to permit storm growth. The median BRN value for southern China (91) is higher than that for northern (58) and central (54) China, and all three of them are higher than those of USSE and USC, reflecting weaker shears. The values of BRN in China range from 34 to 117 for the middle 50% of cases, with a median of 56. About 50% of China SIGTOR have BRN values that exceed the approximate upper limit of 50 as suggested by Weisman and Klemp (1982), mainly because of the low vertical wind shear. On the other hand, the BRN values of many cases in USSE do not satisfy the lower limit because of strong low-level shear. The BRN of USC is most favorable for supercells (Weisman and Klemp, 1982), consistent with the fact that tornadic storms in the region are most supercells (Duda and Gallus 2010) (Fig. 12a). For USSE

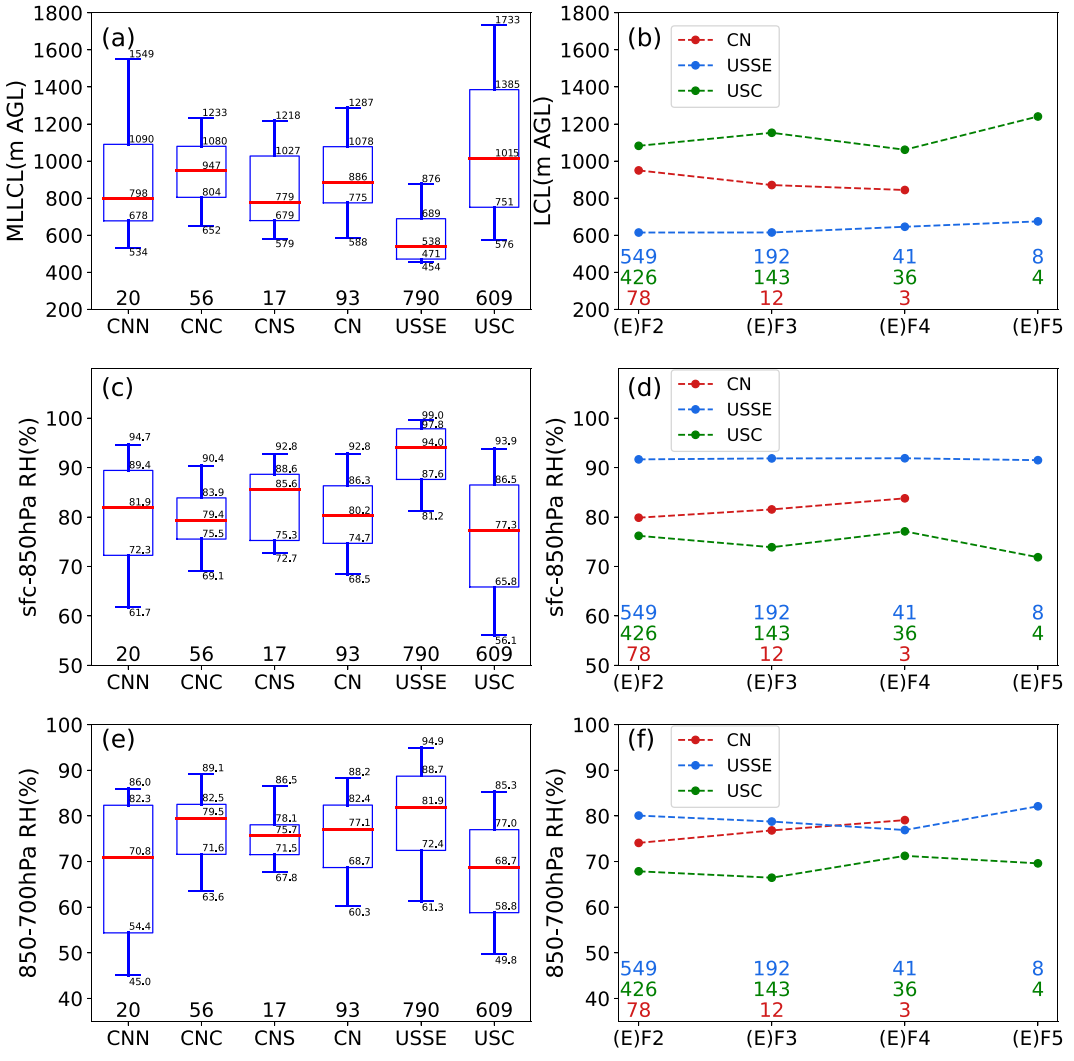

FIG. 10. As in Fig. 5, but for MLLCL, low-level (surface–850 hPa) average relative humidity, and midlevel (850–700 hPa) average relative humidity.

and USC, there is not much change in BRN with tornado intensity, whereas in China there is a slight negative correlation (Fig. 12b); the latter appears to be mainly due to shear increase for (E)F4 tornadoes, but its sample size is very small.

The denominator of BRN is the BRN shear (Table 2). Here we use SR6km to approximate the BRN shear following RB98. The SIGTOR of China, USSE and USC are plotted in the parameter space of surface-based CAPE (SBCAPE) and SR6km in Fig. 12c. China SIGTOR on average occur with moderate SBCAPE and the lowest SR6km among the three regions. USSE SIGTOR occur with the lowest SBCAPE and the highest SR6km while USC SIGTOR occur with the highest SBCAPE and moderate-to-high SR6km. The black curves denote constant BRN values in the space. Most cases in USSE have BRN lower than 10, most cases in USC have BRN lower than 50 while a larger percentage of cases in China have BRN exceeding 50.

Energy-helicity index EHI1 is the product of CAPE and SRH1 (Table 2). Consistent with the slightly monotonic decreasing trend of SRH1 and CAPE from northern to southern China shown in Figs. 7a and 8a, the distribution of EHI1 also decreases from northern China to southern China (Fig. 13a). Rasmussen (2003) suggested that EHI1 values greater than 1–2 are associated with SIGTOR in supercells. One-half of cases in China (~52%), and most of the cases in USSE (~62%) and USC (~66%) have EHI1 $\geq$ 1. As with BRN, China SIGTOR are generally found at moderate CAPE and lowest SR6km than U.S. cases (Fig. 13c). About half of China samples are located above the EHI1 = 1 line, as are most U.S. cases. Unlike BRN, the likelihoods of SIGTOR in all three regions increase with increasing EHI1, as shown in Fig. 13b, suggesting EHI1 being a much better predictor for tornado intensity, even better than SRH1 (cf. Fig. 7b).

Composed of 0–4-km mean shear and CAPE (Table 2), VGP measures the rate of conversion of horizontal environmental vorticity to vertical vorticity through tilting, so higher values indicate stronger mesocyclone (RB98). The relative

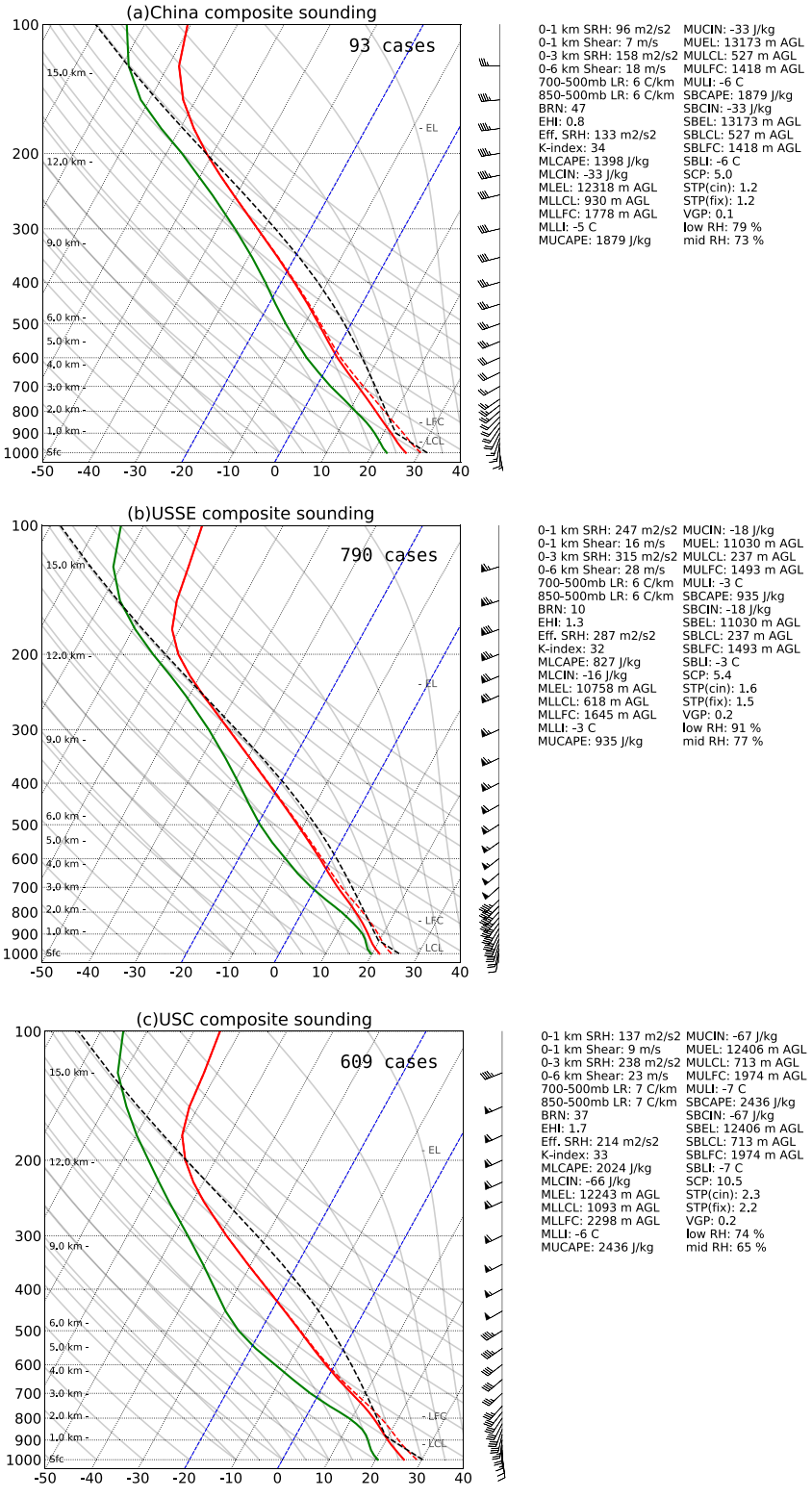

FIG. 11. Regional composite soundings of (a) CN (93 cases), (b) USSE (790 cases), and (c) USC (609 cases). Solid red, solid green, dashed red, and dashed black lines denote temperature, dewpoint, virtual temperature, and parcel trace. Dashed blue lines denote 0° and −20°C isotherms. The composite wind profile for each region is the average of individual wind profiles after their 0–6-km shear vector is aligned with the mean 0–6-km shear vector.

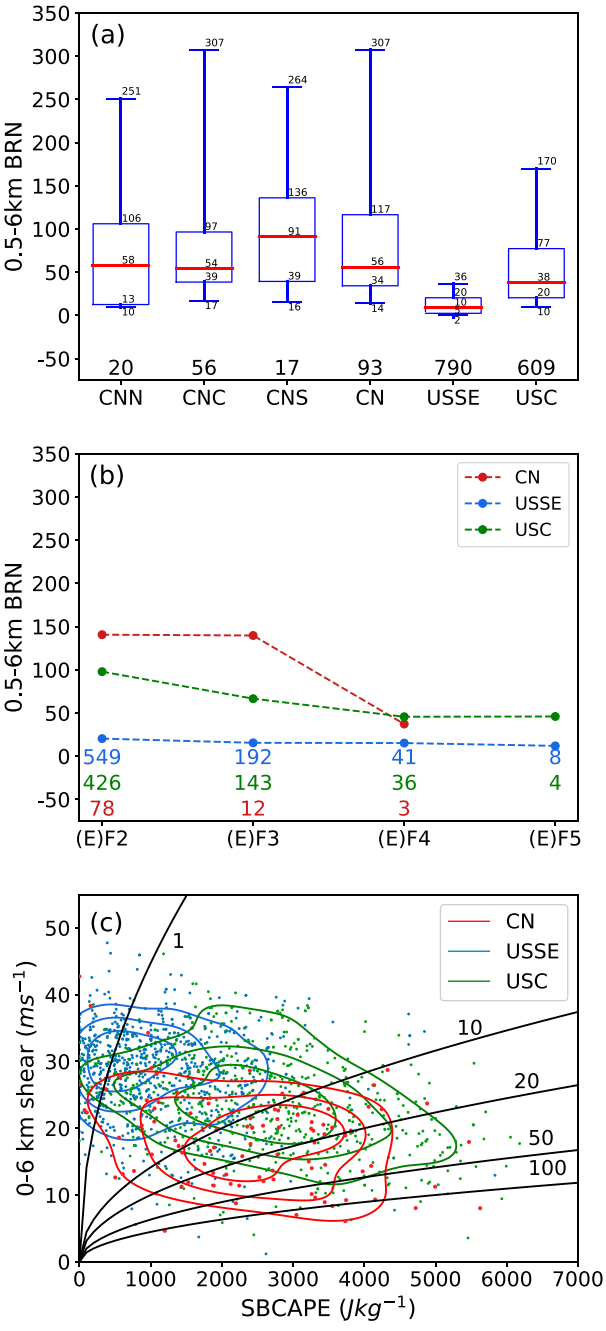

FIG. 12. (a),(b) As in Fig. 5, but for BRN. Also shown is (c) SBCAPE–SR6km parameter space distributions of SIGTOR in CN (red), USSE (blue), and USC (green). Labeled curves are lines of constant BRN. Each set of contours is centered on the location of highest density of events, with the innermost contour enveloping 25% of the data, and contours enveloping 50% and 75% of the data as one moves outward. A Gaussian kernel is used for the kernel density estimation, which serves to smooth the distribution.

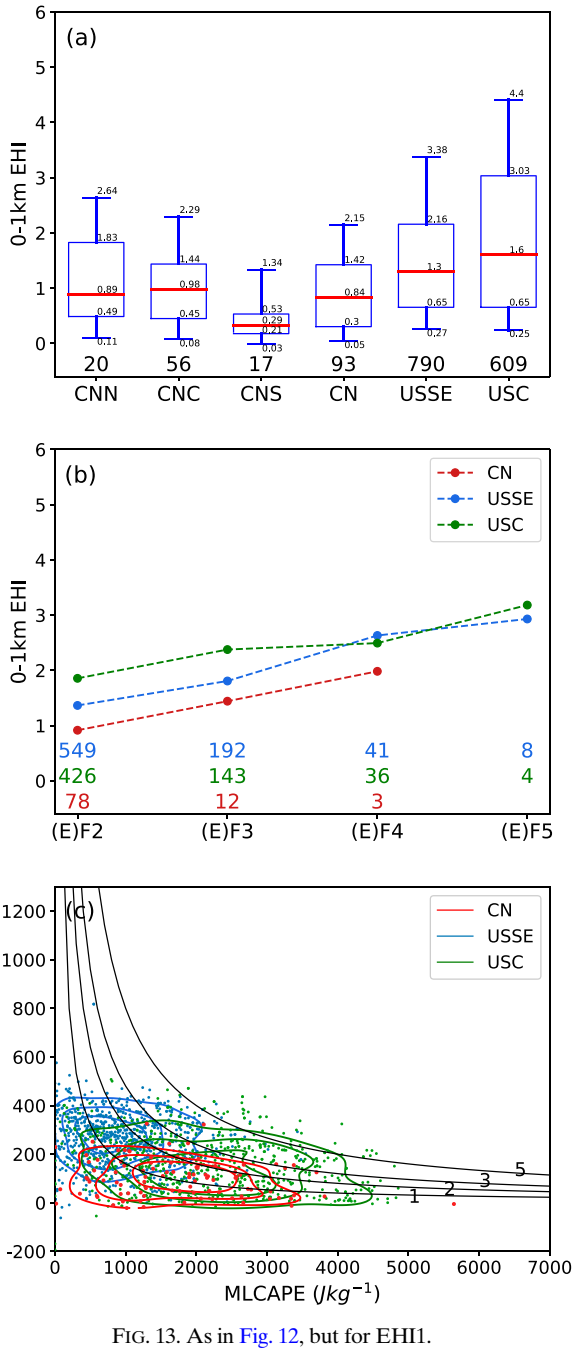

FIG. 13. As in Fig. 12, but for EHI1.

distributions of the regions are similar to those of EHI1 (Fig. 14), since VGP is also the product of a kinematic parameter related to vertical shear and CAPE (Fig. 14a). The values of China VGP extend from 0.105 to 0.193 for the middle 50% of samples with a median of 0.145. As with BRN and EHI1, the red contours representing higher densities of China SIGTOR are considerably displaced toward moderate CAPE and lower shear than the equivalent densities of U.S. counterparts within the 0–4-km shear versus CAPE plot (Fig. 14c). Some USC cases with VGP > 0.3 largely distinguish the inflow environments of SIGTOR occurring in USC and the other two regions, indicating a higher tilting rate in USC. Also, VGP increases with increasing tornado intensity for all three regions (Fig. 14b), similar to EHI1 (Fig. 13b).

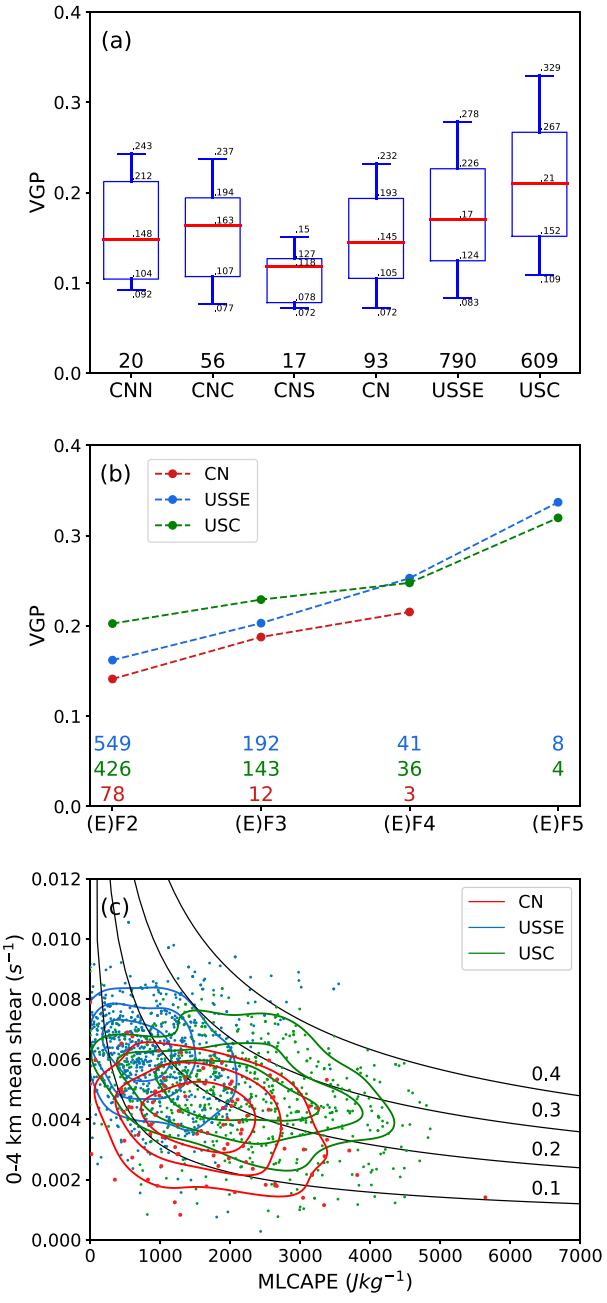

FIG. 14. As in Fig. 12, but for VGP.

In addition to the combined parameters consisting of two parameters discussed above, supercell composite parameter (SCP) and significant tornado parameter (STP) combine more individual parameters; they have been formulated to identify environments that support supercells and to distinguish between tornadic and nontornadic supercells, respectively (Thompson and Hart 2002). STPC, which contains an additional term related to CIN, can reduce areal false alarms (Thompson et al. 2011) and is another form of STP. We focus on the distributions of these parameters in China, USSE, and USC. The average SCP values in all three regions exceed 6, which is reasonably consistent with RB98. More than one-half of the USC samples have SCP $>$ 10, while the majority of events in China have SCP $<$ 10 (Fig. 15a). Overall, CAPE and shear terms contribute the most to SCP. For the USSE SCP, the contribution of the SRH term is more important while for the USC SCP, both CAPE, and SRH are important. Though the CAPE term contributes positively to the China SCP, the smaller SRH term leads to relatively low values of China SCP, confirming the results based on single parameters in section 4a. STP and SCP have similar most influential components (Fig. 16a). By plotting the distributions of individual terms within the composite parameters, the negative contribution to STP of the SRH term below 1 for China and of the CAPE term below 1 for USSE are evident while relatively large SRH terms of USSE and USC make the STP values of corresponding regions large (Fig. 16a). Also, the bulk shear BWD term reduces the China STPC (Fig. 17a). For each rating, the mean values of SCP, STP, and STPC in China are the lowest, indicating less favorable environmental conditions for SIGTOR there. The mean values are highest in USC. Like EHI and VGP, stronger tornadoes tend to occur with increasing SCP, STP, and STPC (Figs. 15b, 16b, and 17b), and the increasing tread is most prominent with STPC, suggesting its best ability in discriminating between (E)F2 and (E)F4 tornadoes. It is noteworthy that this result is more robust for the U.S. tornado dataset, since only three (E)F4 and 0 (E)F5 tornadoes exist in the China tornado dataset.

5. Summary

The purpose of this study is to compare the distributions of environmental parameters of tornadoes occurring in two representative regions of the United States with those occurring in China. A sample of 129 significant tornadoes [SIGTOR, tornadoes rated (E)F2+] in China, 796 in the southeast United States (USSE, including Mississippi, Alabama, and Georgia), and 616 in the central United States (USC, including Oklahoma and the part of Texas north of Dallas) is collected over a 37-yr period from January 1980 to December 2016. None of tornadoes in China was rated (E)F5, and only 3 (E)F4 cases had been recorded in China in the period. Both frequency and intensity of SIGTOR in China are significantly lower than those of the United States.

The number of SIGTOR in China fluctuates through the years, with an overall decreasing trend in the 37 years. The seasonal and diurnal cycles of SIGTOR in China are evident, with a major peak in summer (July), a minor peak in spring (April) and a diurnal peak in the afternoon (1500–1700 BJT). Following earlier climatology studies (Chen et al. 2018; Zheng 2020), we divided China into three regions, North, central, and South China. Northern and central China show similar monthly variations as whole China, and southern China peaks in April related to the northward progression of Asian summer monsoon from the spring. In USSE, cold-season and nighttime SIGTOR account for 56% and 44% of all occurrences, higher than those in China and USC. The diurnal variation in SIGTOR frequency in USSE is less prominent because SIGTOR there occur throughout the day, showing

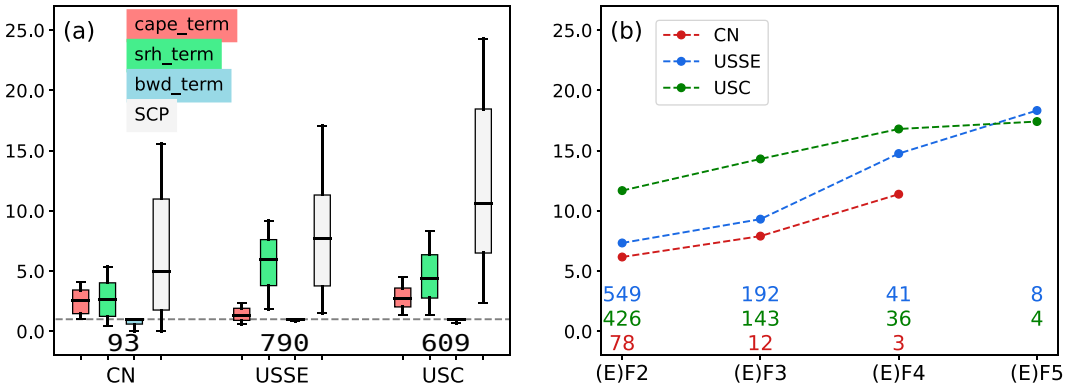

FIG. 15. (a) Box-and-whisker graph of SCP. Three different clusters represent CN, USSE, and USC. Red, green, blue, and white boxes denote the CAPE, SRH, and BWD terms and the SCP, and the dashed line is for value 1. The limits of the box are the 25th and 75th percentiles, and the whiskers extend to the 10th and 90th percentiles. The numbers of samples for each group are listed below the columns. (b) Variation of the mean of SCP with tornado damage ratings. Red, blue, and green lines denote CN, USSE, and USC, respectively. The numbers of samples for each of the EF ratings for CN (red), USSE (blue), and USC (green) are listed below the columns.

moderate peaks in the afternoon and around midnight. USC exhibits the most evident seasonal and diurnal variations, with tornado frequency peaking in the spring and between 1500 and 2100 CST. Spatially, China SIGTOR mainly occur in the eastern regions with flat terrain, concentrating in the Yangtz–Huaihe River basin, North China Plain, and Hubei and Hunan Provinces. SIGTOR are also found in the southern coastal area and the Northeast Plain.

Further, we calculated 17 parameters to gauge the difference of SIGTOR inflow environments between the China and U.S. regions. It is found that kinematic conditions for China SIGTOR are less favorable than those for the United States, characterized by relatively low vertical wind shear, SRH and wind speed. The instability and humidity conditions of tornadic cases of China are favorable, having moderate-to-high CAPE, low CIN and low LCL as well as moderate-to-high midlevel and low-level relative humidity, due to summer monsoon transporting warm and moist air into China. Because of the mountainous terrain and location near the South China coast, southern China SIGTOR are characterized by low CAPE, weak shear and low LCL, which are characteristic of tropical to subtropical environments. Northern China SIGTOR tend to occur in environment with high shear and high LCL, while central China events that account for majority of China samples tend to occur in environment with moderate shear, CAPE and humidity. In USSE, more SIGTOR occur at nighttime that are coupled with nocturnal LLJ, their SIGTOR environments hence exhibit pronounced high shear. The inflow environments of SIGTOR occurring in USC are characterized by large shear, CAPE, CIN, lapse rates, and high LCL.

Moreover, we examined composite environmental parameters that reflect the combined effect of kinematic and thermodynamic conditions on tornado development. Parameters that combine shear and CAPE (BRN, EHI, and VGP) and parameters that combine multiple parameters (SCP and STP) are calculated. The results indicate that single kinematic parameters related to vertical wind shear have greater ability in distinguishing SIGTOR environments (than thermodynamic parameters) in all three regions. The USC samples fit well the thresholds given by earlier works. Influenced by relatively low CAPE (because of more nighttime samples), the composite parameter values of the USSE cases are lower than those of

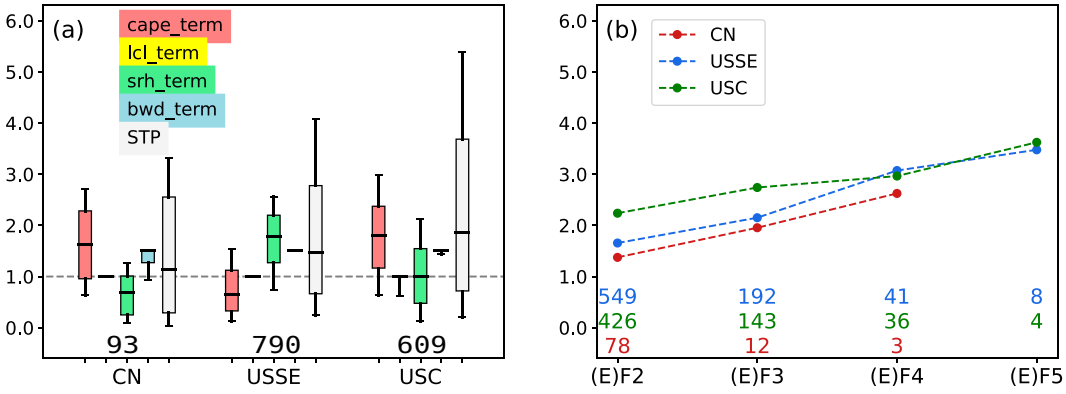

FIG. 16. As in Fig. 15, but for STP. The yellow box denotes the LCL term.

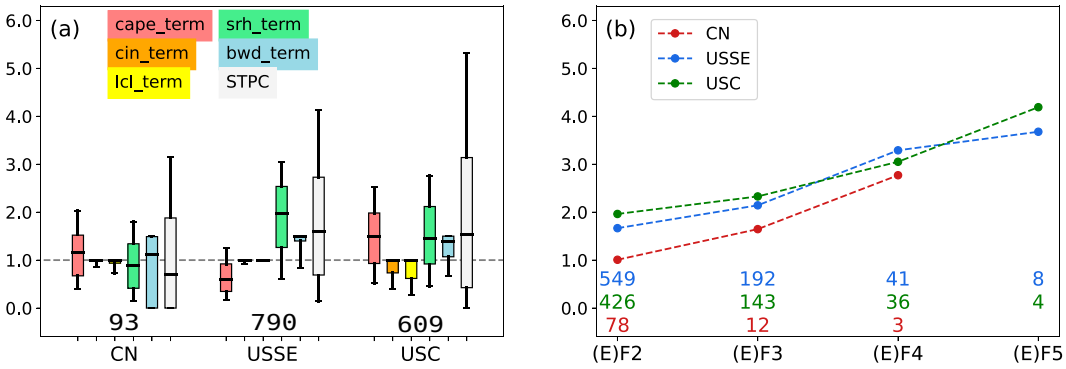

FIG. 17. As in Fig. 15, but for STPC. Yellow and orange boxes denote the LCL and CIN terms, respectively.

the USC cases. Because of less favorable shear conditions, the China SIGTOR environment is characterized by large BRN (many samples have values exceeding the upper bound of BRN = 50 for supercells) and low values of EHI, VGP, STP and SCP (i.e., less favorable for tornado) in comparison with the U.S. regions. The mean value of EHI, VGP, SCP and STP for each rating tends to increase with tornado intensity rating in all three regions, indicating their ability in discriminating tornado intensity. Further studies should verify if the parameters still have sufficient ability to distinguish between tornadic and nontornadic storms in China and if the reference and scaling constants in the composite parameters and thresholds for the individual parameters should be adjusted to improve their predictive capability. Future studies should also extend the length of samples in China and examine representative cases in different regions in more detail.

Acknowledgments. This work was primarily supported by NSFC Grant 41730965 and National Key Research and Development Program of China (2018YFC1507303). The ERA5 reanalysis dataset was downloaded online (https://cds.climate.copernicus.eu/). The tornado data of the U.S. regions were downloaded from the SPC website (https://www.spc.noaa.gov/wcm/index.html#data).

Data availability statement. The software used in this research is available online (https://github.com/sharppy/SHARPpy). The processed data used in this paper can be found at Harvard Dataverse (https://dataverse.harvard.edu/dataset.xhtml?persistentId=doi:10.7910/DVN/L8PXVX).

REFERENCES

Anderson-Frey, A. K., Y. P. Richardson, A. R. Dean, R. L. Thompson, and B. T. Smith, 2016: Investigation of near-storm environments for tornado events and warnings. *Wea. Forecasting*, **31**, 1771–1790, https://doi.org/10.1175/WAF-D-16-0046.1.

——, ——, ——, ——, and ——, 2019: Characteristics of tornado events and warnings in the southeastern United States. *Wea. Forecasting*, **34**, 1017–1034, https://doi.org/10.1175/WAF-D-18-0211.1.

Ashley, W. S., A. J. Krmenec, and R. Schwantes, 2008: Vulnerability due to nocturnal tornadoes. *Wea. Forecasting*, **23**, 795–807, https://doi.org/10.1175/2008WAF2222132.1.

Bai, L., and Coauthors, 2017: An integrated damage, visual, and radar analysis of the 2015 Foshan, Guangdong, EF3 tornado in China produced by the landfalling Typhoon Mujigae (2015). *Bull. Amer. Meteor. Soc.*, **98**, 2619–2640, https://doi.org/10.1175/BAMS-D-16-0015.1.

——, Z. Meng, K. Sueki, G. Chen, and R. Zhou, 2020: Climatology of tropical cyclone tornadoes in China from 2006 to 2018. *Sci. China Earth Sci.*, **63**, 37–51, https://doi.org/10.1007/s11430-019-9391-1.

Bluestein, H. B., 2013: *Severe Convective Storms and Tornadoes: Observations and Dynamics*. Springer–Praxis, 252 pp.

Blumberg, W. G., K. T. Halbert, T. A. Supinie, P. T. Marsh, R. L. Thompson, and J. A. Hart, 2017: SHARPpy: An open-source sounding analysis toolkit for the atmospheric sciences. *Bull. Amer. Meteor. Soc.*, **98**, 1625–1636, https://doi.org/10.1175/BAMS-D-15-00309.1.

Brooks, H. E., C. A. Doswell III, and J. Cooper, 1994: On the environments of tornadic and nontornadic mesocyclones. *Wea. Forecasting*, **9**, 606–618, https://doi.org/10.1175/1520-0434(1994)009<0606:OTEOTA>2.0.CO;2.

——, ——, and M. P. Kay, 2003: Climatological estimates of local daily tornado probability for the United States. *Wea. Forecasting*, **18**, 626–640, https://doi.org/10.1175/1520-0434(2003)018<0626:CEOLDT>2.0.CO;2.

Brown, R. A., 1993: A compositing approach for preserving significant features in atmospheric profiles. *Mon. Wea. Rev.*, **121**, 874–880, https://doi.org/10.1175/1520-0493(1993)121<0874:ACAFPS>2.0.CO;2.

Cai, K., X. Yu, C. Li, X. Huang, L. Yan, Q. He, W. Mai, and Z. Chen, 2021: Comparative analysis of damage survey of microburst in Lingui of Guangxi and tornado in Zhanjiang of Guangdong in 2019 (in Chinese with English abstract). *Meteor. Mon.*, **47**, 230–241, https://doi.org/10.7519/j.issn.1000-0526.2021.02.009.

Carlson, T. N., S. G. Benjamin, G. S. Forbes, and Y.-F. Li, 1983: Elevated mixed layers in the regional severe storm environment: Conceptual model and case studies. *Mon. Wea. Rev.*, **111**, 1453–1474, https://doi.org/10.1175/1520-0493(1983)111<1453:EMLITR>2.0.CO;2.

Chen, J., and Coauthors, 2018: Tornado climatology of China. *Int. J. Climatol.*, **38**, 2478–2489, https://doi.org/10.1002/joc.5369.

Coffer, B. E., M. D. Parker, R. L. Thompson, B. T. Smith, and R. E. Jewell, 2019: Using near-ground storm relative helicity

in supercell tornado forecasting. *Wea. Forecasting*, **34**, 1417–1435, https://doi.org/10.1175/WAF-D-19-0115.1.

——, M. Taszarek, and M. D. Parker, 2020: Near-ground wind profiles of tornadic and nontornadic environments in the United States and Europe from ERA5 reanalyses. *Wea. Forecasting*, **35**, 2621–2638, https://doi.org/10.1175/WAF-D-20-0153.1.

Colby, F. P., Jr., 1984: Convective inhibition as a predictor of convection during AVE-SESAME II. *Mon. Wea. Rev.*, **112**, 2239–2252, https://doi.org/10.1175/1520-0493(1984)112<2239:CIAAPO>2.0.CO;2.

Coleman, T. A., and P. G. Dixon, 2014: An objective analysis of tornado risk in the United States. *Wea. Forecasting*, **29**, 366–376, https://doi.org/10.1175/WAF-D-13-00057.1.

Concannon, P. R., H. E. Brooks, and C. A. Doswell III, 2000: Climatological risk of strong to violent tornadoes in the United States. Preprints, *Second Symp. on Environmental Applications*, Long Beach, CA, Amer. Meteor. Soc., 9.4, https://ams.confex.com/ams/annual2000/techprogram/paper_6471.htm.

Craven, J. P., and H. E. Brooks, 2004: Baseline climatology of sounding derived parameters associated with deep, moist convection. *Natl. Wea. Dig.*, **28**, 13–24, https://www.nssl.noaa.gov/users/brooks/public_html/papers/cravenbrooksnwa.pdf.

——, R. E. Jewell, and H. E. Brooks, 2002: Comparison between observed convective cloud-base heights and lifting condensation level for two different lifted parcels. *Wea. Forecasting*, **17**, 885–890, https://doi.org/10.1175/1520-0434(2002)017<0885:CBOCCB>2.0.CO;2.

Davies, J. M., 1993: Hourly helicity, instability, and EHI in forecasting supercell tornadoes. Preprints, *17th Conf. on Severe Local Storms*, Saint Louis, MO, Amer. Meteor. Soc., 107–111.

Davis, J. M., and M. Parker, 2014: Radar climatology of tornadic and nontornadic vortices in high-shear, low-CAPE environments in the mid-Atlantic and southeastern United States. *Wea. Forecasting*, **29**, 828–853, https://doi.org/10.1175/WAF-D-13-00127.1.

Davies-Jones, R. P., 1984: Streamwise vorticity: The origin of updraft rotation in supercell storms. *J. Atmos. Sci.*, **41**, 2991–3006, https://doi.org/10.1175/1520-0469(1984)041<2991:SVTOOU>2.0.CO;2.

——, D. Burgess, and M. Foster, 1990: Test of helicity as a forecast parameter. Preprints, *16th Conf. on Severe Local Storms*, Kananaskis Park, AB, Canada, Amer. Meteor. Soc., 50–60.

Ding, Y., 2008: *The Collection of Meteorological Disasters Records in China* (in Chinese). Meteorological Press, 948 pp.

Doswell, C. A., III, and E. N. Rasmussen, 1994: The effect of neglecting the virtual temperature correction on CAPE calculations. *Wea. Forecasting*, **9**, 625–629, https://doi.org/10.1175/1520-0434(1994)009<0625:TEONTV>2.0.CO;2.

Duda, J. D., and W. A. Gallus, 2010: Spring and summer Midwestern severe weather reports in supercells compared to other morphologies. *Wea. Forecasting*, **25**, 190–206, https://doi.org/10.1175/2009WAF2222338.1.

Efron, B., and R. J. Tibshirani, 1993*: An Introduction to the Bootstrap*. Chapman and Hall, 436 pp.

Fan, W., and X. Yu, 2015: Characteristics of spatial-temporal distribution of tornadoes in China (in Chinese with English abstract). *Meteor. Mon.*, **41**, 793–805.

Garner, J. M., 2012: Environments of significant tornadoes occurring within the warm sector versus those occurring along surface baroclinic boundaries. *Electron. J. Severe Storms Meteor.*, **7** (5), https://ejssm.org/archives/2012/vol-7-5-2012/.

Grams, J. S., R. L. Thompson, D. V. Snively, J. A. Prentice, G. M. Hodges, and L. J. Reames, 2012: A climatology and comparison of parameters for significant tornado events in the United States. *Wea. Forecasting*, **27**, 106–123, https://doi.org/10.1175/WAF-D-11-00008.1.

Guyer, J. L., and A. R. Dean, 2010: Tornadoes within weak CAPE environments across the continental United States. *25th Conf. on Severe Local Storms*, Denver, CO, Amer. Meteor. Soc., 1.5, https://ams.confex.com/ams/25SLS/webprogram/Paper175725.html.

Hart, J. A., and W. Korotky, 1991: The SHARP workstation v 1.50 users guide. NOAA/NWS Doc., 30 pp.

Henson, R., 2003: Twisting around the world. *Weatherwise*, **56**, 14–20, https://doi.org/10.1080/00431670309605383.

Hersbach, H., and Coauthors, 2020: The ERA5 global reanalysis. *Quart. J. Roy. Meteor. Soc.*, **146**, 1999–2049, https://doi.org/10.1002/qj.3803.

Hurlbut, M. M., and A. E. Cohen, 2014: Environments of northeast U.S. severe thunderstorm events from 1999 to 2009. *Wea. Forecasting*, **29**, 3–22, https://doi.org/10.1175/WAF-D-12-00042.1.

Kelly, D. L., J. T. Schaefer, R. P. McNulty, C. A. Doswell III, and R. F. Abbey Jr., 1978: An augmented tornado climatology. *Mon. Wea. Rev.*, **106**, 1172–1183, https://doi.org/10.1175/1520-0493(1978)106<1172:AATC>2.0.CO;2.

Kerr, B. W., and G. L. Darkow, 1996: Storm-relative winds and helicity in the tornadic thunderstorm environment. *Wea. Forecasting*, **11**, 489–505, https://doi.org/10.1175/1520-0434(1996)011<0489:SRWAHI>2.0.CO;2.

Kis, A. K., and J. M. Straka, 2010: Nocturnal tornado climatology. *Wea. Forecasting*, **25**, 545–561, https://doi.org/10.1175/2009WAF2222294.1.

Krocak, M. J., and H. E. Brooks, 2018: Climatological estimates of hourly tornado probability for the United States. *Wea. Forecasting*, **33**, 59–69, https://doi.org/10.1175/WAF-D-17-0123.1.

Lilly, D. K., 1986: The structure, energetics and propagation of rotating convective storms. Part II: Helicity and storm stabilization. *J. Atmos. Sci.*, **43**, 126–140, https://doi.org/10.1175/1520-0469(1986)043<0126:TSEAPO>2.0.CO;2.

Long, J. A., P. C. Stoy, and T. Gerken, 2018: Tornado seasonality in the southeastern United States. *Wea. Climate Extremes*, **20**, 81–91, https://doi.org/10.1016/j.wace.2018.03.002.

Maddox, R. A., 1976: An evaluation of tornado proximity wind and stability data. *Mon. Wea. Rev.*, **104**, 133–142, https://doi.org/10.1175/1520-0493(1976)104<0133:AEOTPW>2.0.CO;2.

Markowski, P. M., and Y. Richardson, 2011: *Mesoscale Meteorology in Midlatitudes*. John Wiley and Sons, 430 pp.

——, J. M. Straka, and E. N. Rasmussen, 2002: Direct surface thermodynamic observations within the rear-flank downdrafts of nontornadic and tornadic supercells. *Mon. Wea. Rev.*, **130**, 1692–1721, https://doi.org/10.1175/1520-0493(2002)130<1692:DSTOWT>2.0.CO;2.

McCaul, E. W., 1991: Buoyancy and shear characteristics of hurricane–tornado environments. *Mon. Wea. Rev.*, **119**, 1954–1978, https://doi.org/10.1175/1520-0493(1991)119<1954:BASCOH>2.0.CO;2.

Meng, Z., and Coauthors, 2018: The deadliest tornado (EF4) in the past 40 years in China. *Wea. Forecasting*, **33**, 693–713, https://doi.org/10.1175/WAF-D-17-0085.1.

Moncrieff, M. W., and M. J. Miller, 1976: The dynamics and simulation of tropical cumulonimbus and squall lines. *Quart. J. Roy. Meteor. Soc.*, **102**, 373–394, https://doi.org/10.1002/qj.49710243208.

Nixon, C. J., and J. T. Allen, 2022: Distinguishing between hodographs of severe hail and tornadoes. *Wea. Forecasting*, **37**, 1761–1782, https://doi.org/10.1175/WAF-D-21-0136.1.

Novlan, D. J., and W. M. Gray, 1974: Hurricane-spawned tornadoes. *Mon. Wea. Rev.*, **102**, 476–488, https://doi.org/10.1175/1520-0493(1974)102<0476:HST>2.0.CO;2.

Potvin, C. K., K. L. Elmore, and S. J. Weiss, 2010: Assessing the impacts of proximity sounding criteria on the climatology of significant tornado environments. *Wea. Forecasting*, **25**, 921–930, https://doi.org/10.1175/2010WAF2222368.1.

Rasmussen, E. N., 2003: Refined supercell and tornado forecast parameters. *Wea. Forecasting*, **18**, 530–535, https://doi.org/10.1175/1520-0434(2003)18<530:RSATFP>2.0.CO;2.

——, and D. O. Blanchard, 1998: A baseline climatology of sounding-derived supercell and tornado forecast parameters. *Wea. Forecasting*, **13**, 1148–1164, https://doi.org/10.1175/1520-0434(1998)013<1148:ABCOSD>2.0.CO;2.

——, K. Laws, R. Morss, and Y. Richardson, 2017: VORTEX-SE science plan. NOAA/NSSL, 63 pp., http://www.nssl.noaa.gov/projects/vortexse.

Reames, L. J., 2017: Diurnal variations in severe weather forecast parameters of Rapid Update Cycle-2 tornado proximity environments. *Wea. Forecasting*, **32**, 743–761, https://doi.org/10.1175/WAF-D-16-0029.1.

Schultz, L. A., and D. J. Cecil, 2009: Tropical cyclone tornadoes, 1950–2007. *Mon. Wea. Rev.*, **137**, 3471–3484, https://doi.org/10.1175/2009MWR2896.1.

Sherburn, K. D., and M. D. Parker, 2014: Climatology and ingredients of significant severe convection in high-shear, low-CAPE environments. *Wea. Forecasting*, **29**, 854–877, https://doi.org/10.1175/WAF-D-13-00041.1.

——, ——, J. R. King, and G. M. Lackmann, 2016: Composite environments of severe and nonsevere high-shear, low-CAPE convective events. *Wea. Forecasting*, **31**, 1899–1927, https://doi.org/10.1175/WAF-D-16-0086.1.

Stackpole, J. D., 1967: Numerical analysis of atmospheric soundings. *J. Appl. Meteor. Climatol.*, **6**, 464–467, https://doi.org/10.1175/1520-0450(1967)006<0464:NAOAS>2.0.CO;2.

Taszarek, M., J. T. Allen, T. Púčik, K. A. Hoogewind, and H. E. Brooks, 2020: Severe convective storms across Europe and the United States. Part II: ERA5 environments associated with lightning, large hail, severe wind, and tornadoes. *J. Climate*, **33**, 10 263–10 286, https://doi.org/10.1175/JCLI-D-20-0346.1.

Thompson, R. L., 2020: Explanation of SPC severe weather parameters. NOAA, accessed 17 January 2022, https://www.spc.noaa.gov/exper/mesoanalysis/help/begin.html.

——, R. Edwards, and J. A. Hart, 2002: Evaluation and interpretation of the supercell composite and significant tornado parameters at the Storm Prediction Center. Preprints, *21st Conf. on Severe Local Storms*, San Antonio, TX, Amer. Meteor. Soc., J3.2, https://ams.confex.com/ams/SLS_WAF_NWP/techprogram/paper_46942.htm.

——, ——, ——, K. L. Elmore, and P. Markowski, 2003: Close proximity soundings within supercell environments obtained from the rapid update cycle. *Wea. Forecasting*, **18**, 1243–1261, https://doi.org/10.1175/1520-0434(2003)018<1243:CPSWSE>2.0.CO;2.

——, ——, and C. M. Mead, 2011: An update to the supercell composite and significant tornado parameters. *22nd Conf. on Severe Local Storms*, Norman, OK, Amer. Meteor. Soc., P8.1, http://ams.confex.com/ams/pdfpapers/82100.pdf.

——, B. T. Smith, A. R. Dean, and P. T. Marsh, 2014: Spatial distributions of tornadic near-storm environments by convective mode. *Electron. J. Severe Storms Meteor.*, **8** (5), https://www.spc.noaa.gov/publications/thompson/ej-env.pdf.

Trapp, R. J., S. A. Tessendorf, E. S. Godfrey, and H. E. Brooks, 2005: Tornadoes from squall lines and bow echoes. Part I: Climatological distribution. *Wea. Forecasting*, **20**, 23–34, https://doi.org/10.1175/WAF-835.1.

Wang, S., and W. Li, 2007*: Climate of China* (in Chinese). China Meteorological Press, 428 pp.

Wang, X., X. Yu, and X. Zhou, 2015: Study of Northeast China torandoes: The environmental characteristics (in Chinese with English abstract). *Acta Meteor. Sin.*, **73**, 425–441.

Weisman, M. L., and J. B. Klemp, 1982: The dependence of numerically simulated convective storms on vertical wind shear and buoyancy. *Mon. Wea. Rev.*, **110**, 504–520, https://doi.org/10.1175/1520-0493(1982)110<0504:TDONSC>2.0.CO;2.

Xue, M., K. Zhao, M. Wang, Z. Li, and Y. Zheng, 2016: Recent significant tornadoes in China. *Adv. Atmos. Sci.*, **33**, 1209–1217, https://doi.org/10.1007/s00376-016-6005-2.

Yu, X., J. Zhao, and W. Fan, 2021: Tornadoes in China: Spatio-temporal distribution and environmental characteristics (in Chinese with English abstract). *J. Trop. Meteor.*, **37**, 681–692.

Zhao, K., and Coauthors, 2017: Doppler radar analysis of a tornadic miniature supercell during the landfall of Typhoon Mujigae (2015) in South China. *Bull. Amer. Meteor. Soc.*, **98**, 1821–1831, https://doi.org/10.1175/BAMS-D-15-00301.1.

Zheng, Y. G., 2020: Review of climatology and favorable environmental conditions of tornado in China (in Chinese with English abstract). *Adv. Meteor. Sci. Technol.*, **10**, 69–75.

——, and Coauthors, 2016: Wind speed scales and rating of the intensity of the 23 June 2016 tornado in Funing County, Jiangsu province (in Chinese with English abstract). *Meteor. Mon.*, **42**, 1289–1303.

Zhou, R., Z. Meng, and L. Bai, 2021: Differences in tornado activities and key tornadic environments between China and the United States. *Int. J. Climatol.*, **42**, 367–384, https://doi.org/10.1002/joc.7248.

Zucchini, W., 2003: *Applied Smoothing Techniques. Part 1: Kernel Density Estimation*. Temple University, 20 pp.